Univerzita Karlova

Přírodovědecká fakulta

Studijní program: Chemie

Studijní obor: Medicinální chemie

Jáchym Hrušák

Návrh a syntéza sloučenin cílených na buněčné jádro pro použití v bioortogonálních reakcích

Design and synthesis of cell nucleus-targeted compounds for use in bioorthogonal reactions

Bakalářská práce

Vedoucí závěrečné práce/Školitel: Ing. Milan Vrábel Ph.D.

Praha, 2022

Prohlášení:

Prohlašuji, že jsem závěrečnou práci zpracoval samostatně a že jsem uvedl všechny použité informační zdroje a literaturu. Tato práce ani její podstatná část nebyla předložena k získání jiného nebo stejného akademického titulu.

V Praze, 19.5.2022

Podpis

Abstrakt

Tato bakalářská práce se soustředí na návrh a syntézu 1,2,4,5-tetrazinových a *trans*--cyklooktenových derivátů s funkčními skupinami schopnými cílit na buněčné jádro a účastnit se bioortogonálních reakcí. Na základě literární rešerše byly navrženy funkční skupiny a struktura tetrazinových a *trans*-cyklooktenových derivátů tak, aby bylo dosaženo selektivního cílení do jádra buněk a aby byla zajištěna dostatečná reaktivita výsledných konjugátů v biologickém prostředí. Takto navržené látky byly syntetizovány a v modelových systémech byly zkoumány jejich vlastnosti a reaktivita.

Klíčová slova: bioortogonální reakce, tetrazin, *trans*-cyklookten, Hoechst, jádro, buňka, akridin, kumarin

Abstract

This bachelor thesis focuses on the design and synthesis of 1,2,4,5-tetrazine and *trans*-cyclooctene derivatives containing functional moieties which are able to target cellular nucleus and participate in bioorthogonal reactions. Based on literature research, the targeting moieties and the structure of the tetrazine and *trans*-cyclooctene derivatives were designed with the aim to achieve selective nuclear targeting and to ensure sufficient reactivity of the resulting conjugates under biological conditions. Selected candidates were then synthesized and their properties together with cellular reactivity were investigated in model experiments.

Key words: bioorthogonal reaction, tetrazine, *trans*-cyclooctene, Hoechst, nucleus, cell, acridine, coumarin

Table of Contents

List of abbreviations used in the text

Ac – acyl

AcOEt – Eethyl acetate

ATP – adenosine triphosphate

Boc – *tert*-Butyloxycarbonyl

CuAAC – copper(I)-catalyzed azide-alkyne cycloaddition

d – doublet

DCM – dichloromethane

DIC – *N*,*N*′-dDiisopropylcarbodiimide

diMeTz – 3,6-dimethyl-1,2,4,5-tetrazine

DMF – *N*′,*N*′-dimethylformamide

DNA – deoxyribonucleic acid

ER – endoplasmic reticulum

Et – ethyl

GA – Golgi apparatus

HBTU – 2-(1*H*-benzotriazol-1-yl)-1,1,3,3-tetramethyluronium hexafluorophosphate

HPLC-MS – High performance liquid chromatography with mass spectrometer

HRMS – high resolution mass spectroscopy

IEDDA – inverse electron-demand Diels-Alder reaction

m – multiplet

Me - methyl

NHS – *N*-hydroxysuccinimide

NLS – Nuclear localization sequence

NMR – nuclear magnetic resonance

PBS – phosphate-buffered saline

ROS – reactive oxygen species

SPAAC – strain-promoted azide-alkyne cycloaddition

TCO – *trans*-cyclooctene

TFA – trifluoroacetic acid

THF – tetrahydrofuran

VdU – 5-vinyl-2′-deoxyuridine

s – singlet

1. Introduction

Bioorthogonal chemistry is a set of methods which employ the chemistry of non-native functional groups in order to investigate the biology in living organisms. Bioorthogonal reactions are reactions that proceed selectively with sufficient kinetics under physiological conditions.[1]

This thesis focuses mainly on the synthesis and reactions of 1,2,4,5-tetrazine derivatives with *trans*-cyclooctenes (TCOs). Tetrazines and TCOs react rapidly under physiological conditions upon release of N_2 molecule to form a stable product (Scheme 1).[2] This reaction belongs to the so-called click reactions and it has found numerous applications especially in chemical biology.[3]

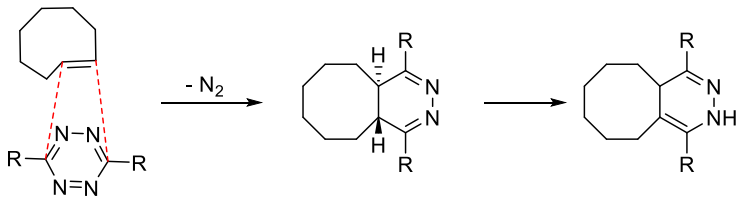

Scheme 1: The click reaction of 1,2,4,5-tetrazine with TCO

Another emerging application of the reaction is based on the release of a biologically active molecule (i.e., drug) upon the reaction of a tetrazine and TCO. Some allyl-substituted TCOs have the ability to release the substituent (drug) upon clicking with a tetrazine. This process is called a click-to-release reaction.[4]

With the click-to-release reaction, there is a growing potential for controlling the release of biologically active molecules by external stimuli. It makes sense to use these reactions in situations where the specificity of the drug by itself is very low or when it is too toxic to be administered to the whole body. The concept of organelle targeting opens a new window for improvement. It is possible to conjugate a drug with a specific moiety that delivers the drug to an organelle of choice (depending on the moiety). By doing so, it is possible to improve the therapeutic index of drugs for example, by increasing the local concentration at the site of action.[5]

In this thesis, I focused on the synthesis of bioorthogonal reagents that have affinity to the cell nucleus and enable labeling and release of molecules in this organelle.

2. Aims and objectives

The aims and objectives of my bachelor thesis are:

a) To conduct theoretical research on the possibilities and use of tetrazine and *trans*-cyclooctene derivatives in bioorthogonal chemistry.
b) To synthesize the candidate compounds.
c) To characterize the synthesized compounds (NMR, HRMS).
d) To investigate the reactivity of the candidate tetrazine-TCO reagents in model release experiments.
e) To investigate the affinity of the synthesized molecules towards the cell nucleus.

3. Bioorthogonal reactions

3.1 What are bioorthogonal reactions?

Bioorthogonal reactions are a set of reactions that neither interact nor interfere with a biological system. Bioorthogonal chemistry moves the environment in which a synthetic reaction is performed from a laboratory to cells and living organisms. The intended purpose of bioorthogonal chemistry is the covalent modification of biomolecules to allow their study and manipulation. Such reactions must obey certain rules for them to be considered bioorthogonal. They must:

- occur under physiological environments
- form products selectively
- be unaffected by endogenous functional moieties
- be fast, even at low concentrations, and form stable products

Therefore, the bioorthogonal functional groups must not be endogenous to the examined systems in order for them to satisfy the above-mentioned rules.[1]

Bioorthogonal chemistry might be confused with the broader field of click chemistry. There is a huge overlap between these two fields, but click chemistry also includes reactions of functional moieties found in biological systems. One example of a 'click chemistry reaction' that does not meet the definition of a bioorthogonal reaction could be the selective protein modification via cysteine alkylations and conjugate additions.[6]

3.2 Examples and evolution of bioorthogonal chemistry

3.2.1 The Staudinger ligation

There are many types of bioorthogonal reactions. The first such reaction introduced to the world is the Staudinger ligation. It is based on the well-known Staudinger reaction where an azide reacts with a phosphine to form an iminophosphorane which oxidizes upon formation of an amine and a phosphine oxide (Scheme 2). The reaction can be modified by introducing an electrophilic trap in the phosphine derivative (Scheme 3). This causes the aminophosphine in **III** to react with the trap (i.e. methyl ester) rather than being hydrolyzed upon formation of an amide bond in **V**.[7] The reaction found many uses in the modification of proteins and other biomolecules, such as nucleic acids.[8] Even though the Staudinger ligation was there since the dawn of bioorthogonal chemistry, it is now facing succession from the other methods mainly because of its insufficient kinetics.[6]

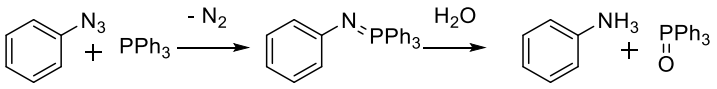

Scheme 2: Staudinger ligation

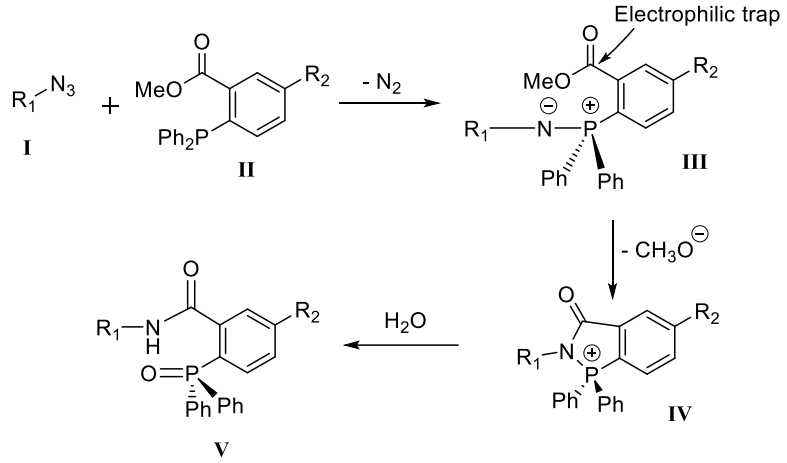

Scheme 3: Staudinger ligation with a methyl ester group acting as an electrophilic trap

3.2.2 Transition metal-catalyzed bioorthogonal reactions

The next big step in bioorthogonal chemistry was the introduction of metal-catalyzed reactions. The first such reaction is the copper(I)-catalyzed azide-alkyne cycloaddition (CuAAC). The reaction, also called the Huisgen reaction, offers 1,4-disubstituted 1,2,3-triazoles (Scheme 4) which act as good mimetics of native peptide bonds.[9] An example of CuAAC use in biological systems is the labeling of glycocalyx's glycoproteins and glycolipids of a cell which was previously presented with azide-containing saccharides. Copper cations are known to be associated with the formation of reactive oxygen species (ROS) and are thereby cytotoxic, which affects the 'true' bioorthogonality of CuAAC. This problem can be partially addressed by introducing specific ligands that stabilize the Cu(I) oxidative state and accelerate the cycloaddition reaction, thus preventing copper from taking part in inducing oxidative stress.[10]

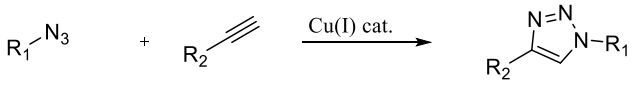

Scheme 4: Copper-catalyzed azide-alkyne cycloaddition

Other possible transition metals with use in bioorthogonal chemistry are either palladium[11] or ruthenium[12].

3.2.3 Strain-promoted azide-alkyne cycloaddition (SPAAC)

Due to the aforementioned imperfections of CuAAC, a new method arose – the strain-promoted azide-alkyne cycloaddition (SPAAC). Two years after the CuAAC was introduced[13,14], this new method came without the need of catalysis and often with very favorable kinetics. It relies on the reaction between an azide and a highly strained alkyne (mostly cyclooctyne) as shown in Scheme 5.[15]

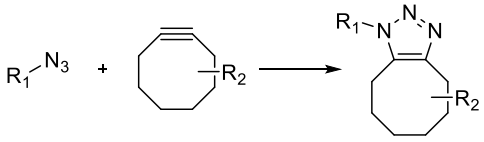

Scheme 5: SPAAC reaction of an azide and a cyclooctyne

3.2.4 Inverse electron-demand Diels-Alder reactions

The inverse electron-demand Diels-Alder (IEDDA) bioorthogonal reaction refers to the tetrazine ligation. It is a cycloaddition reaction between *s*-tetrazine and a dienophile, namely for purposes of this work – *trans*-cyclooctene (TCO). This reaction proceeds with very fast reaction rates without the need of a catalyst and is therefore a suitable candidate for use in bioorthogonal chemistry. The reaction is shown in Scheme 6, and it is important to note that, unlike in the "classical" Diels-Alder reaction, it is a reaction between an electron rich (or strained) dienophile (TCO) and an electron poor heterodiene (tetrazine). TCO derivatives are known to have really good reaction kinetics with tetrazines, apparently due to the strain present in the cycle. In the first step of the reaction, a highly strained bicyclic molecule is formed which undergoes a retro-Diels-Alder reaction upon release of N_2 as the only byproduct.[2]

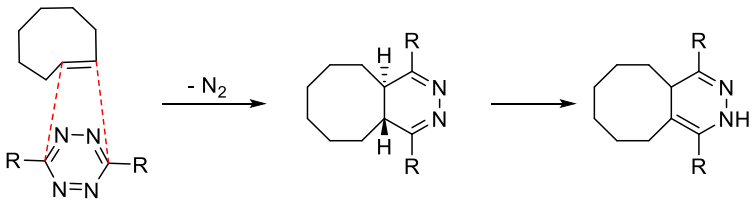

Scheme 6: The IEDDA reaction between a 1,2,4,5-tetrazine derivative and TCO

The reactivity and stability of 1,2,4,5-tetrazines strongly depends on the substituents attached to positions 3 and 6. The main problem for use in biological conditions is the presence of nucleophiles and water. It has been discovered that 3,6-diaryl substituted tetrazines are a good choice for aqueous environment.[2]

3.2.4.1 Tetrazines in drug activation

Prodrugs are the biologically inactive forms of drugs. Their activation was historically provided by enzymes, but due to their lack of selectivity, these procedures commonly came

with undesired side effects. Needless to say, a different method of activating drugs more specifically was craved by the scientific society. Various methods of drug-activating bioorthogonal reactions have been examined over the past two decades, and the outcome is that in terms of kinetics and biocompatibility tetrazine IEDDA reactions are the best choice. Scheme 7 shows that upon treatment of TCO-drug conjugate **VI** with a tetrazine derivative **VII**, the resulting product **VIII** is the same as shown in Scheme 6 (click) but spontaneous electron rearrangement causes the drug's release. This methodology is also called as *click-to-release* reaction.[4] The drug must be localized in the allylic position connected by an oxygen or a nitrogen atom via ether, carbamate or ester bond for the release to take place.[16]

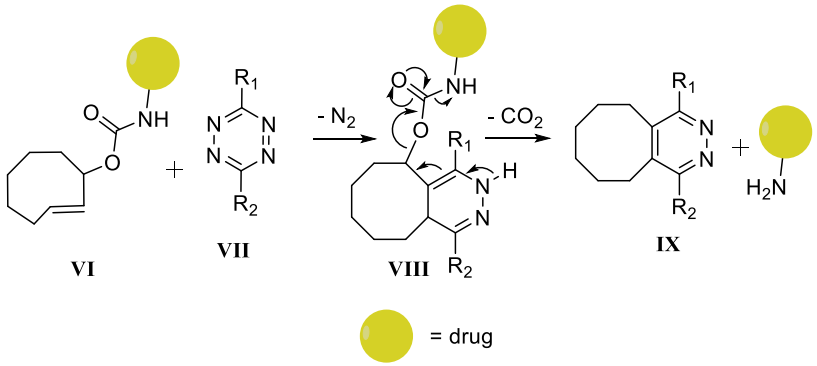

Scheme 7: Tetrazine drug activation with the mechanism of the drug releasing electron transfer

It has been shown in various cases that this type of reaction can be successfully performed *in vivo*, mostly in the treatment of cancer[17–19]. For example, an even "more bioorthogonal" reaction was described in 2018 (lit. 20) and is shown in Scheme 8. It is a tetrazine-mediated prodrug-prodrug activation, where both the strained alkene and the tetrazine are prodrugs which are activated when they are clicked. The tetrazine **X** serves as a microRNA 21 (miR21) inhibitor precursor (miR21 is often closely connected to tumors). The anti-cancer drug camptothecin in **XI** has the alcohol group protected with a vinyl group , which also serves as the bioorthogonal functional moiety that reacts with the tetrazine.

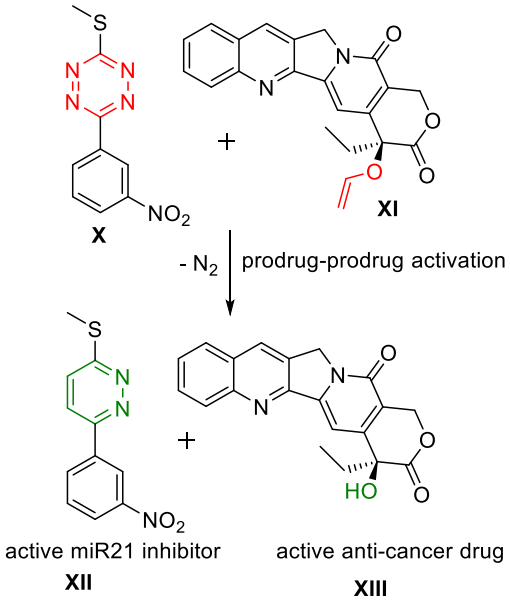

Scheme 8: Tetrazine mediated prodrug-prodrug activation

4. Organelle targeting

Cancer and cancer-like diseases are characterized by invasive cells with uncontrolled and undifferentiated proliferation and sometimes metastasis – the spread of the cancer cells throughout the body via blood or lymph. One of the main approaches in treatment of these diseases is chemotherapy, other ones being radiation or surgery. Due to their relatively low specificity towards cancer cells, chemotherapeutic agents show, to some extent, cytotoxicity towards healthy cells. To counter the nonspecific distribution, new strategies constantly evolve with the aim to specifically target desired (cancerous) cells while minimizing the impact on the healthy ones, thus increasing the drug's therapeutic index. A widely used and popular example of such strategy is the conjugation of chemotherapeutic agents to monoclonal antibodies, which bind specifically to receptors that are abundant or exclusive for the target cells. It is possible to take these thoughts to another level and concentrate on the fate of the therapeutic agent after it has reached the desired cell and tends to a specific organelle – subcellular targeting. The two main goals of subcellular targeting are minimizing the required amount of a therapeutic agent and, most importantly, overcoming the multidrug resistance which is one of the most common problems in cancer treatment.[5]

4.1 Mitochondria

Mitochondria are widely known for their production of energy in the form of adenosine triphosphate (ATP). Their role is much broader than that, including the generation of reactive oxygen species (ROS), cell signaling or apoptosis. The dysfunction of mitochondria is associated with many diseases such as obesity or cancer.[21] Unlike most other cells, cancer cells rely mostly on glycolysis even in aerobic conditions. This is called the Warburg effect.[22] Even though they produce most of their ATP from glycolysis, cancer cell mitochondria maintain high membrane potential. This is explored in modern cell targeting strategies.

Most recent studies use the greatly negative membrane potential of mitochondria to drive the molecules towards them. Such molecules are therefore positively charged.[23–25] In 1999, for example, vitamin E (antioxidant) was successfully delivered to mitochondria by coupling it with triphenylphosponium cation.[26]

4.2 Lysosomes

Lysosomes are organelles with a single membrane involved in degradation of macromolecules. Their pH is acidic which is generated by ATP-dependent H^+ pumps. They

contain many enzymes (mostly hydrolases) which help the degradation of various macromolecules.[5] Many diseases (Danon disease, Farber disease) are associated with the dysfunction of lysosomes and subsequent accumulation of undegraded materials. More and more evidence show that there is a direct link between lysosomes and Alzheimer's disease or cancer.[27]

Proteins (enzymes) can get to lysosomes either by merging with endosomes or via autophagy. During autophagy, organelles are degraded by lysosomes in the event of cell starvation.[28] The main targeting signal for proteins destined for lysosomes is D-mannose-6-phosphate. Only proteins tagged with D-mannose-6-phosphate are then recognized by receptors in the Golgi apparatus and forwarded to lysosomes. This is a precautionary measure to ensure that lysosomal enzymes aren't present freely in the cytosol.[29] This tagging technique is used to direct proteins to lysosomes in the event of lysosome dysfunction more specifically lysosomal storage diseases, such as Gaucher's disease.[30]

Another method of visualizing lysosomes is the use of acridine orange (Fig. 1).[31]
One other method of targeting lysosomes was described in 2016 that served for visualization of cathepsin-B which is a lysosomal protease and it appears to be an important biomarker for many malignant tumors. The lysosome locating group (Fig. 1) contains a morpholine ring with a short lipophilic chain.[32]

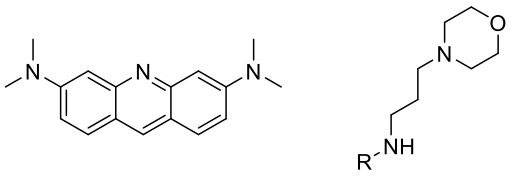

Figure 1: Lysosome locating groups – acridine orange (left) and morpholine-based locating group (right)

4.3 Golgi apparatus

Golgi apparatus (GA) is the central organelle of the secretory pathway of the cell. It performs posttranslational modifications on proteins using enzymes. Such modifications include phosphorylation, acylation, glycosylation, and others. For example, mannose-6-phosphate can be added to a protein to direct it to lysosome, as mentioned in the section above.[5] Dysfunction of the Golgi apparatus may lead to several neurodegenerative disorders including Parkinson's, Alzheimer's or amyotrophic lateral sclerosis.[33]

4.4 Endoplasmic reticulum

Endoplasmic reticulum's (ER) primary function is to facilitate the folding of secretory and membrane proteins, lipid biosynthesis and Ca^{2+} storage. Several diseases are linked with ER, such as coagulation factor X deficiency or hypothyroidism. Recent studies have shown that ER can be linked to cancer. It seems to play an integral role in cancer aggressiveness, metastasis, and response to chemotherapy.[34]

Several strategies for targeting the ER have been developed. Molecules that tend to accumulate in this organelle are usually of an amphipathic character and moderately lipophilic nature. Two such molecules are shown in Fig. 2.[35]

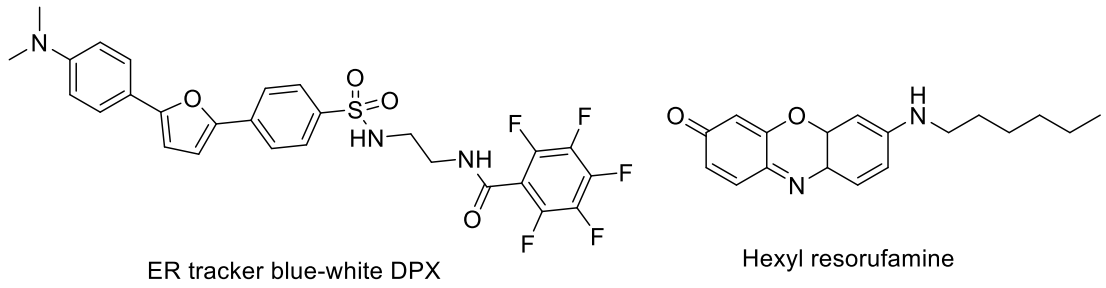

Figure 2: Molecules with reported tendency to accumulate in the ER

4.5 Nuclear targeting

Nucleus controls the function of the eukaryotic cell. It does so by controlling the gene expression and other cellular mechanisms mediated by selective translocation of proteins between nucleus and cytoplasm.[5] Access to the cell nucleus is controlled by the nuclear envelope, which is comprised of a double-layered membrane perforated with nuclear pores that regulate passage of proteins in and out of the nucleoplasm, but are relatively permeable to small molecules.[36]

One method of nuclear targeting is inspired by oligopeptide tags used by DNA viruses in order to insert their genetic material to host cell viruses. Such peptides are known as nuclear localization sequences (NLSs). They are short peptide sequences rich in lysine, arginine and proline which have the ability to translocate molecules attached to them through the nuclear pores. First NLS to be discovered was the Simian virus 40 NLS (Fig. 3).[36]

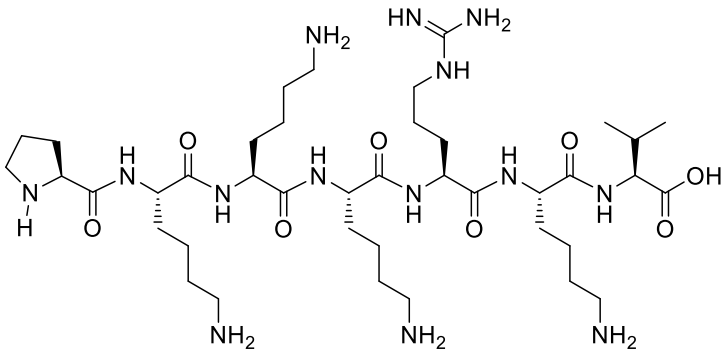

Figure 3: Simian virus 40 NLS (PKKKRKV)

Another method is the use of fluorescent dyes, such as Hoechst or DAPI which have the ability to bind DNA. For DNA staining, incubation with Hoechst dye is usually the go-to method due to simplicity, low cost, and no requirements for genetic modification. Hoechst also has greater cell permeability and lower cytotoxicity than other available dyes.

The name Hoechst refers to a group of bisbenzimide dyes with differently numbered derivatives (Hoechst 33258, Hoechst 33342, Hoechst 34580) as shown in Fig. 4.

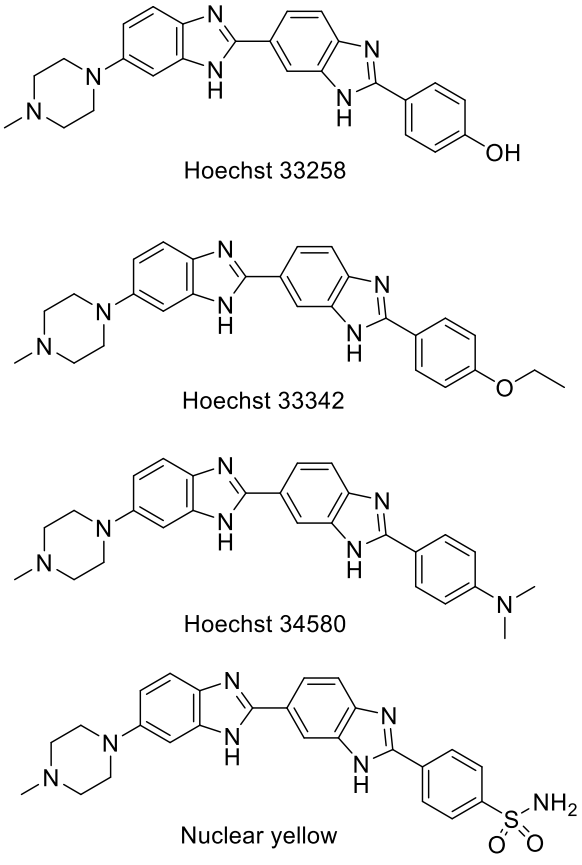

Figure 4: Various commercially available Hoechst dyes

They carry the name of the German company Hoechst AG that started in the early 1970s.[37] Hoechst dyes are excited by UV light at around 360 nm, and they emit a broad spectrum of blue light with the maximum in the 460 nm region. Their important property is that their fluorescence increases ~30-fold upon binding to DNA, which causes a good signal-to-noise ratio. The increase of fluorescence is caused by the suppression of rotational relaxation and the reduction of hydration when bound to DNA.[38]

Hoechst dyes bind to the minor groove of DNA in adenine(A) thymine(T) rich regions with a very low cytotoxic effect. Even slight changes in the molecular structure of the dye can cause big changes in the accumulation in the cells, e.g. Hoechst 33342 accumulates 10x as much in the cells compared to Hoechst 33258. One problem of the dyes is the phototoxicity of UV light[39], which is necessary for imaging with the conventional Hoechst dyes. In 2010, Hoechst-IR (Fig. 5) was described in the context of in vivo imaging of necrotic cells, which are a hallmark of various diseases including cancer. The purpose of such a molecule is not to travel to the nucleus. Instead, it binds to the extracellular DNA which is released after a necrotic cell death to the extracellular space.[40]

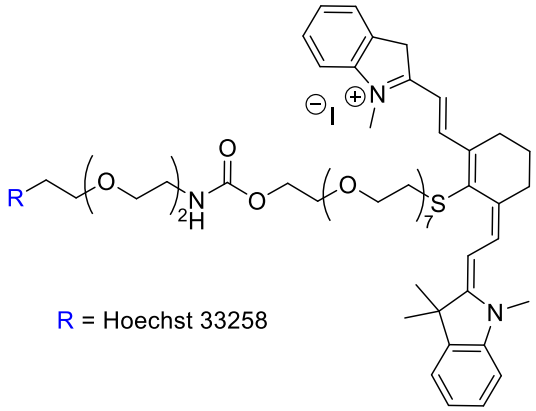

Figure 5: Hoechst-IR

Due to aforementioned low cytotoxicity, high affinity to DNA and a good cell permeability, Hoechst dyes have the potential to act as DNA-targeting molecules in drug development. One example of such use is the conjugation of the anti-cancer drug Gemcitabine with Hoechst 33258 – H-Gemcitabine (Fig. 6). Gemcitabine is by itself a drug with great clinical potential, but it is limited by its relatively high toxicity and inactivation in serum. H-Gemcitabine, however, is protected from the inactivation in blood stream and it accumulates inside tumors by binding to the present extracellular DNA. The Gemcitabine is then released by slow hydrolysis whereupon it starts to actively kill the tumor cells. It should also be mentioned that the H-Gemcitabine conjugate is cell-impermeable which results in decreased systemic toxicity in comparison to free Gemcitabine.[41]

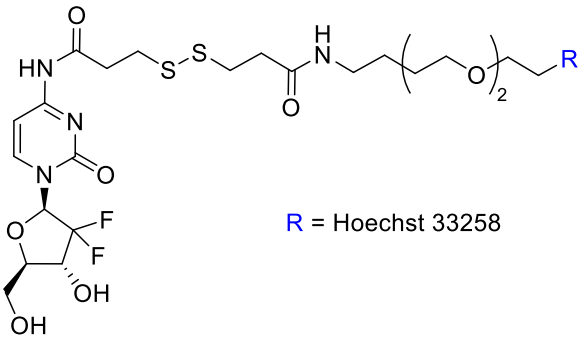

Figure 6: Hoechst-Gemcitabine conjugate

5. Results and discussion

5.1 Synthesis of tetrazine-Hoechst conjugate

The first objective of this thesis was to synthesize a tetrazine derivative **2** in the form of an active ester to be ready for subsequent coupling reactions with amines. The inspiration for the tetrazine **2** came from recent works[42,43] showing good results in terms of bioorthogonality, stability and sufficient kinetics of this particular derivative.

Hoechst dyes have an affinity to the cell nucleus and become fluorogenic upon interaction with DNA as discussed in the Chapter 4.5. Tetrazines, in turn, participate in bioorthogonal reactions with strained alkenes (such as TCO). The conjugate of the two compounds should have properties of both the compounds and is therefore a good candidate for use in nucleus-targeted bioorthogonal reactions.

The first step was the synthesis of the tetrazine in the form of a carboxylic acid (Scheme 9). A commercially available substance **1** in ethanol was treated with acetonitrile and hydrazine hydrate in the presence of 3-mercaptopropionic acid to yield the reduced form of the desired product.[44] The oxidation is done by sodium nitrate in the presence of HCl as an acid to yield the tetrazine product **2**.

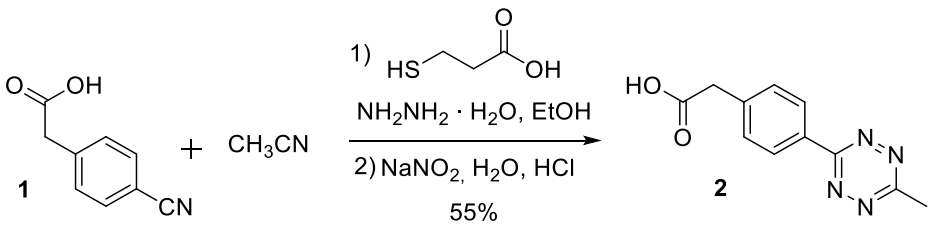

Scheme 9: Synthesis of tetrazine **2**

Subsequently, the active ester form of the tetrazine **2** was synthesized (Scheme 10). This is a standard procedure[42] which produces a substance that readily reacts with nucleophiles (amines in our case) with relatively high yields. The tetrazine **2** was treated with N-hydroxysuccinimide (**NHS**) in the presence of DIC as a coupling reagent. DIC acts by coupling with the carboxylic acid by which a diisopropylurea intermediate forms. Then, a nucleophilic attack on the carboxylic carbon by the NHS takes place which eliminates the diisopropyl urea byproduct. The reaction was performed in THF at 0 °C and the desired product was isolated in 66% yield.

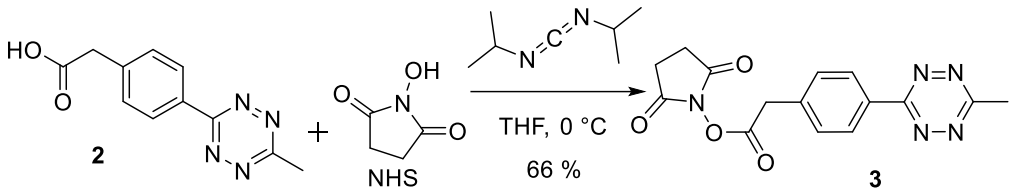

Scheme 10: Synthesis of tetrazine active ester

The next step was the synthesis of Hoechst 33258 derivative **4** with a short lipophilic chain which later served as the linker to the tetrazine moiety. Hoechst 33258 by itself does not have good cell permeability due to the -OH group, that is partially deprotonated under physiological conditions thus making it cell impermeable. This problem can be solved with introduction of a lipophilic linker via an ether bond on the oxygen.

A commercially available Hoechst 33258 was treated with a *tert*-butyloxycarbonyl (Boc) protected 2-bromoethylamine with K_2CO_3 acting as a base, standard conditions for the Williamson ether synthesis as shown in Scheme 11. The mechanism relies on alkoxide formation when the base (K_2CO_3) and the alcohol (Hoechst 33258) react. The anionic form then proceeds to a nucleophilic attack on the brominated hydrocarbon and the bromine, being a good leaving group, departs. The amino group is protected by Boc so it does not participate in the reaction.

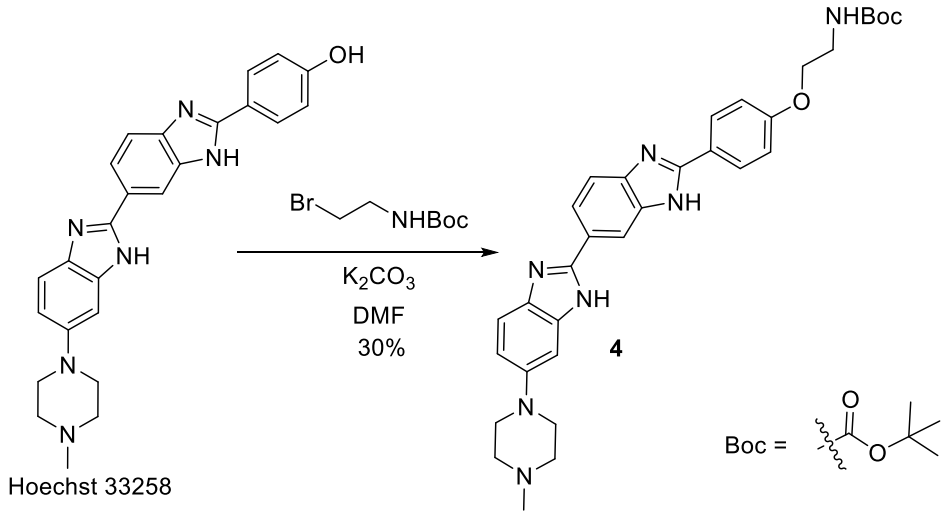

Scheme 11: Synthesis of ether from Hoechst 33258

The following step was the deprotection of the amino group of **4**. This was done by trifluoroacetic acid (TFA) in dichloromethane (DCM) at 0 °C as shown in Scheme 12. The mechanism relies on an acid-mediated cleavage of the tert-butyl cation from the Boc group with subsequent decarboxylation, which leaves us with protonated amine as the product **5**. Then, the

CF_3COO^- counterions were exchanged for acetate ions on Dowex. These deprotections tend to work smoothly and almost quantitatively under these conditions.

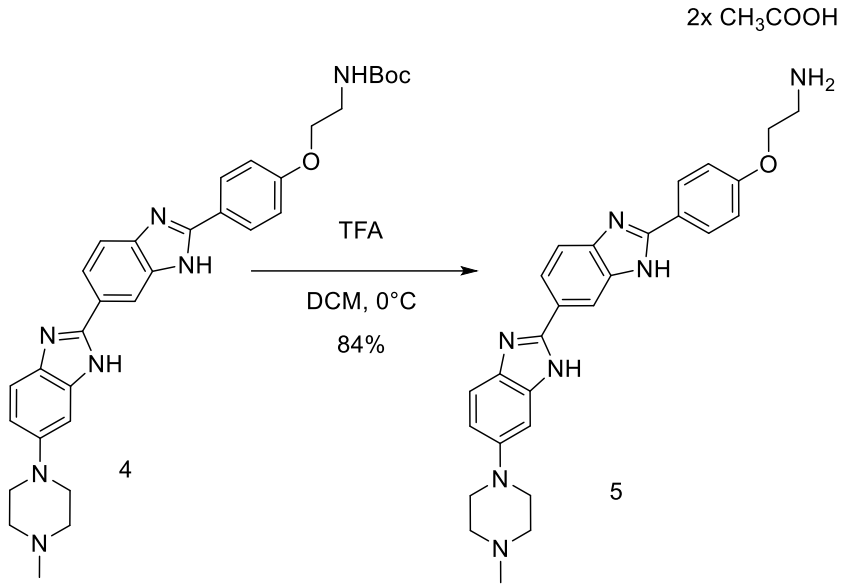

Scheme 12: Hoechst-amine Boc deprotection

The next step was the synthesis of the tetrazine-Hoechst conjugate. As discussed in the chapter 4.4, Hoechst dyes have an intrinsic affinity to the cell nucleus (or rather DNA) where they bind to the minor groove of dsDNA. Tetrazines, in turn, act as bioorthogonal reagents in reactions with strained alkenes (TCO in our case) as discussed in the chapter 3.2.4. This molecule should therefore be able to target the cell nucleus and then click with TCO, which should be observable on the fluorescence properties of this bifunctional conjugate.

The reaction of the amino group of Hoechst **5** and the active ester **3** (Scheme 13) with triethylamine as base proceeded in 56% yield. This rather lower yield can be possibly attributed to the presence of competing cyclic amino groups of the benzimidazole ring that can also react with the NHS active ester. This assumption was supported by the observed of double (and possibly even triple) modified amides of **5** by HPLC-MS analysis.

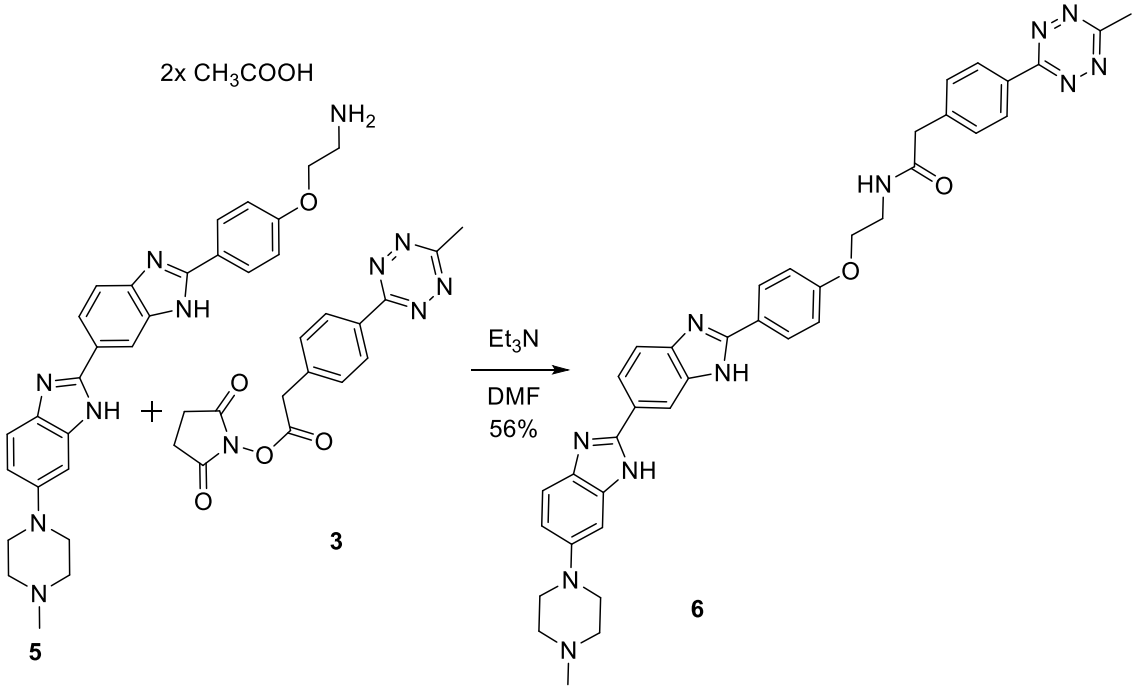

Scheme 13: The conjugation of Hoechst and tetrazine

5.2 Synthesis of tetrazine-morpholine conjugate

With enough of the compound **3** at hand (not all was consumed by the reaction in Scheme 13), we decided to prepare another tetrazine derivative, in this case containing a morpholine. We hypothesized that tetrazine **7** will be a good candidate with possible tendency to accumulate in lysosomes as discussed in the Chapter 4.2. A reaction between active ester **3** and 3-morpholinopropan-1-amine (Scheme 14) gave the desired product **7** with a high yield of 92%.

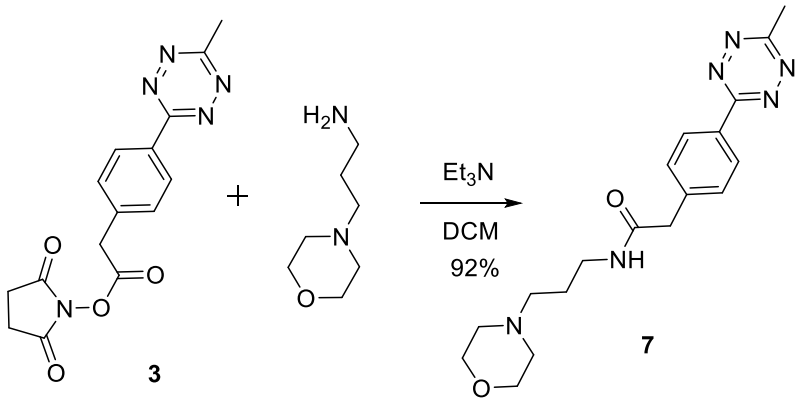

Scheme 14: Synthesis of a tetrazine with lysosomal activity

5.3 Synthesis of TCO derivatives

The next step in the conceptual development of the thesis was the synthesis of TCO derivatives that would later be "clicked" with the synthesized tetrazines. The goal was to prepare a conjugate of TCO with a fluorophore, that would enable us to track the distribution of the Hoechst-tetrazine compounds inside the cells. TCO does not have a quenching effect on fluorescence as some tetrazines do.[45] Therefore, it would make sense to synthesize TCO derivatives with fluorophores of different spectral properties than those of Hoechst dyes. The absorption/emission of such molecules would than depend on the number of molecules "clicked" when presented with the tetrazine-Hoechst conjugate **6**.

The first such TCO derivative was assigned to have coumarin attached as the fluorophore, despite the overlapping spectral properties of the two dyes (coumarin and Hoechst) The reason was a good experience with the use of coumarin dyes in the Vrabel group[46] and availability of the building blocks. Coumarin by itself should not alter the affinity of such molecules to any specific region of the cell, which is an important prerequisite for tracking the molecules inside cells. Therefore, in cellular assays, the molecule should diffuse throughout targeted cells and click with tetrazines wherever they are present. The unclicked molecules of TCO-coumarin conjugate should be washable from the cells and the Hoechst dye from clicked molecules of **6** should have its fluorescence unquenched.

The first step of the synthesis was the formation of a boronic acid derivative **10**. In this reaction, a short lipophilic linker with one Boc- protected amino group **9** was attached onto a carboxy-phenylboronic acid **8** using HBTU as a coupling reagent with pyridine as a base as shown in Scheme 15. The desired intermediate was isolated in 66% yield.

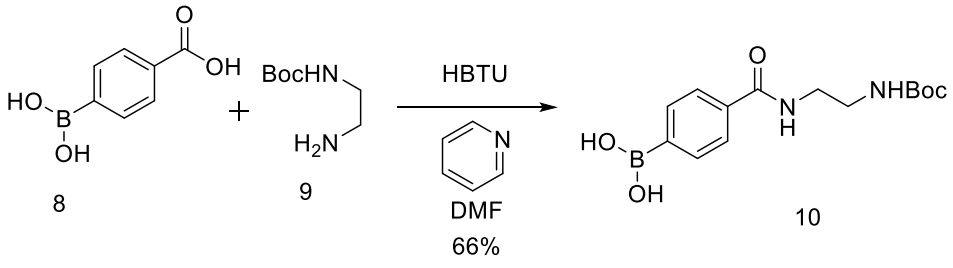

Scheme 15: Connecting a lipophilic chain to boronic acid derivative via an amide bond

The next step of the synthesis was the Suzuki cross-coupling reaction of a coumarin derivative **11**[46] and boronic acid derivative **10** (Scheme 16). This reaction creates a carbon-carbon bond between the two aromatic cycles containing bromine (on **11**) and boronic acid (on **10**) under Pd catalysis. Pd(dppf)Cl_2·DCM was used as a catalyst along with K_2CO_3 as base in dioxane:water 4.5:1 mixture which yielded product **12** in 45% yield.

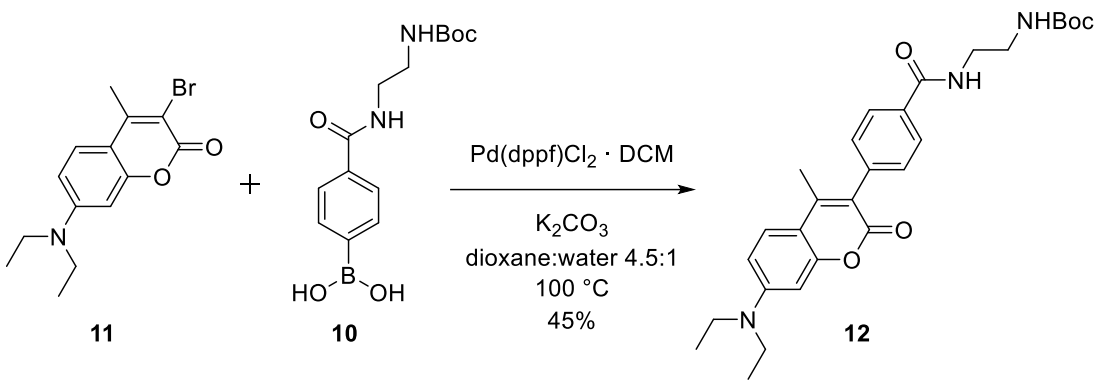

Scheme 16: Suzuki coupling of coumarin derivative

The next reaction was the deprotection of the Boc-protected amine. The reaction was performed under the same conditions as shown in Scheme 12 except for temperature which was here changed for room temperature instead of 0 °C. The reaction product with the deprotected primary amine formed as the corresponding trifluoroacetic salt **13** as shown in Scheme 17. The reaction yield was 87 %.

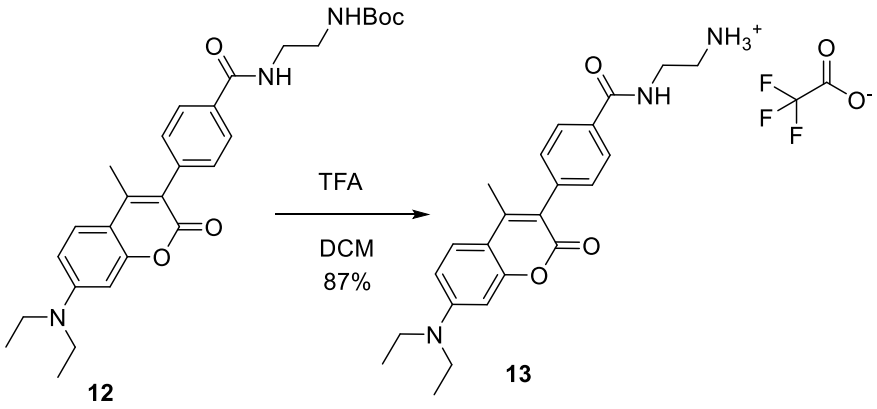

Scheme 17: Coumarin Boc deprotection

With the amino group deprotected, the compound **13** readily reacted with a commercially available active ester of TCO upon formation of **14** as the product with 84% yield. Unfortunately, it was found out from NMR spectrum that ca 50% of *trans*-cyclooctene isomerized into *cis*- configuration, which was also confirmed in a small control reaction with tetrazine and subsequent analysis by HPLC-MS. In this case, only the *trans*-isomer reacts in matter of seconds while the *cis*- one is left untouched. The exact reason for the observed isomerization is not clear at the moment, the highly reactive and strained TCOs are known to undergo *trans*-to-*cis* isomerization under various conditions.[47] Separation of these two isomers was not possible neither on silica gel, nor on reversed phase column. This issue (mixture of two

isomers) was later addressed and considered during the model cellular labeling experiments. The reaction (Scheme 18) was performed in DMF using triethylamine as a base (Scheme 13).

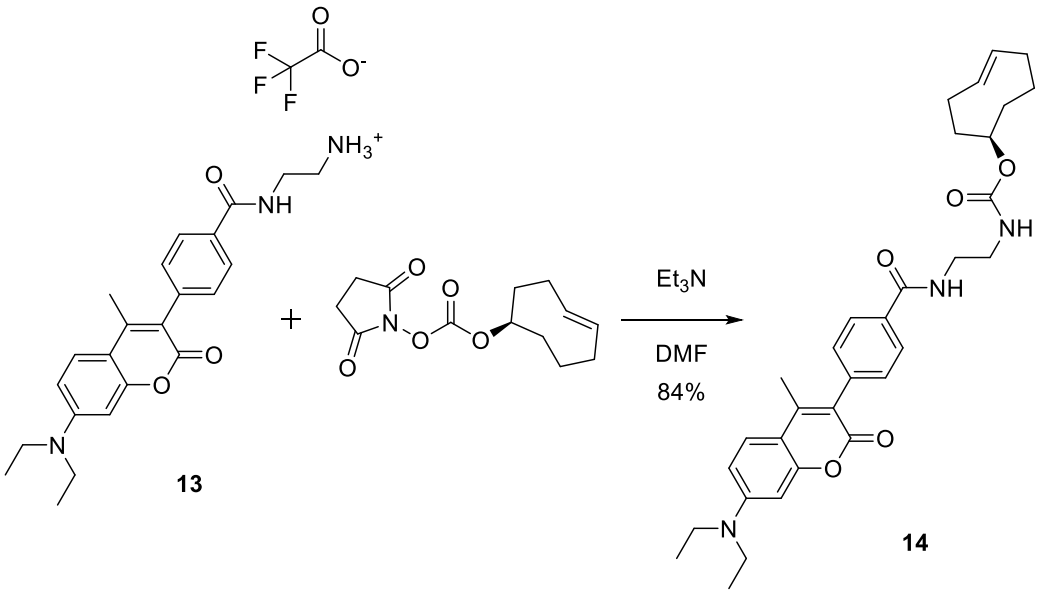

Scheme 18: Coumarin-TCO synthesis

Next, we decided to synthesize Hoechst-TCO conjugate **15** (Scheme 19). Our goal was to prepare this compound in order to evaluate if the Hoechst can serve as a nuclear-targeting moiety also from the 'other' side of the TCO dienophile. For the synthesis, Hoechst precursor **5** reacted with commercial **TCO-NHS** (Scheme 19) under basic conditions and gave the desired Hoechst-TCO product **15** in excellent yield of 80% as 3x HCOOH salt isolated after reversed phase column with 0.05% HCOOH as modifier of mobile phase. Ion exchange on Dowex was then performed to get the compound in the form of the 'more' natural Cl^- salt.

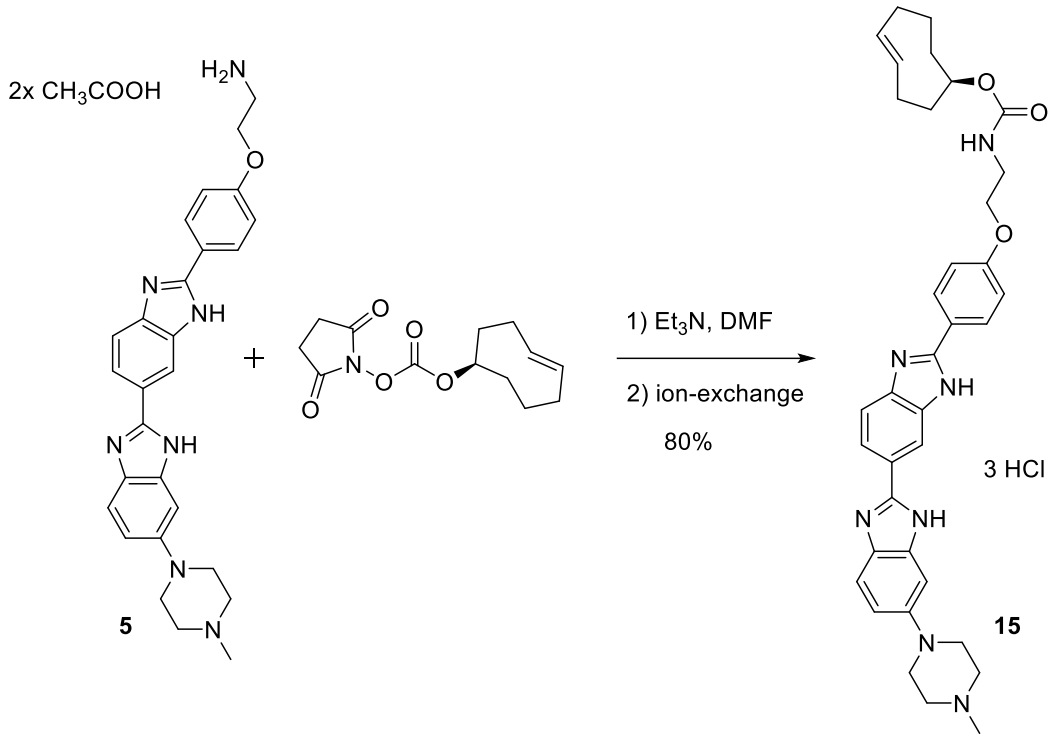

Scheme 19: Synthesis of Hoechst-TCO conjugate

5.4 Synthesis of a tetrazine-acridine conjugate

In a recent article[48] from 2022, a new fluorogenic tetrazine was described to have the spectral properties in line with our outlined goals (Fig. 7). The molecule is able to reversibly intercalate in a dsDNA thanks to the acridine tricycle. The tetrazine serves both as a bioorthogonal functional group and as a fluorescence quencher. The article describes the use of the tetrazine-acridine conjugate as a lighting-up probe enabling monitoring of newly synthesized DNA after metabolic incorporation of 5-vinyl-2'-deoxyuridine (VdU).

In this thesis, I tried to take advantage of the above-mentioned properties. The synthesis of the compounds was done according to the article.

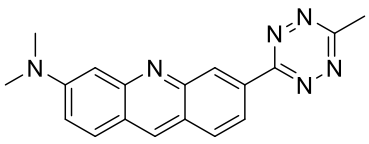

Figure 7: Tetrazine-acridine conjugate

The commercially available dihydrochloride **16a** was converted into free amine[49] **16b** which underwent a Buchwald-Hartwig cross-coupling with commercially available compound **17** (Scheme 20). The resulting secondary amine **18** underwent a spontaneous cyclization mediated by silica gel acting as a weak Lewis acid. The reaction shown in Scheme 20 yielded the acridine nitrile **19** in a 23% yield over 2 steps.

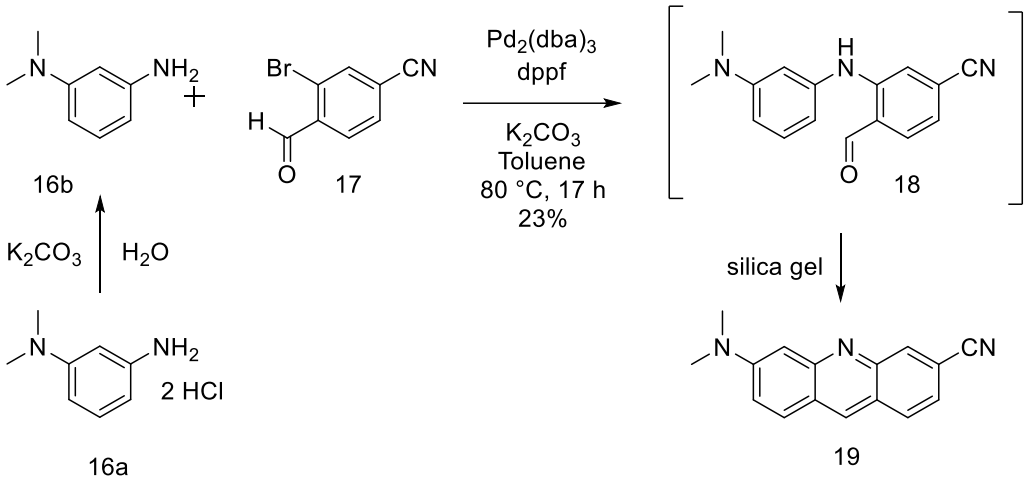

Scheme 20: The synthesis of the acridine nitrile 19

Next, the synthesis of the asymmetric tetrazine **20** was accomplished by treating the acridine nitrile **19** with hydrazine, Zn(II)triflate and acetonitrile followed by oxidation with $NaNO_2$ to give the tetrazine **20** (Scheme 21).

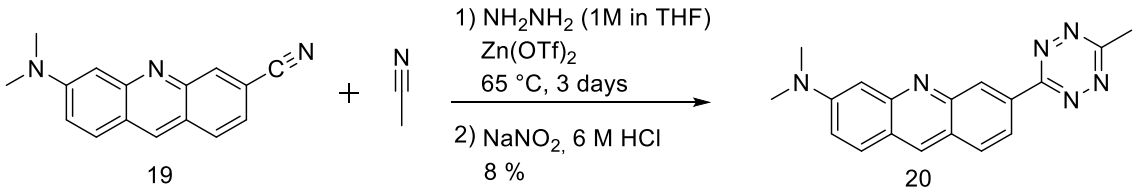

Scheme 21: Synthesis of tetrazine-acridine conjugate

5.5 UV/Vis tetrazine with TCO-Reso decaging experiment

To evaluate the releasing ability of the synthesized tetrazines, an experiment based on the release of the fluorescent resorufin was performed. Resorufin is a well-established fluorophore being used in many biological assays. The compound **21** (TCO-Reso) used for the experiments consists of a TCO attached in the allylic position to resorufin dye via *N*,*N*′-dimethylethylenediamine spacer. The TCO-caged resorufin serves in this case as a reporter molecule enabling monitoring of the click to release process by following changes in the absorption or fluorescence spectra.

The TCO moiety reacts with the tetrazine to form the clicked product **22**. Then, a spontaneous electron rearrangement causes the release of the spacer with resorufin **23**. The *N*,*N*′-dimethylethylenediamine spacer is a commonly used self-immolative linker, so a spontaneous cyclisation causes the loss of an urea byproduct with concomitant release of free resorufin **24** as the product.[50] The mechanism is shown in Scheme 22.

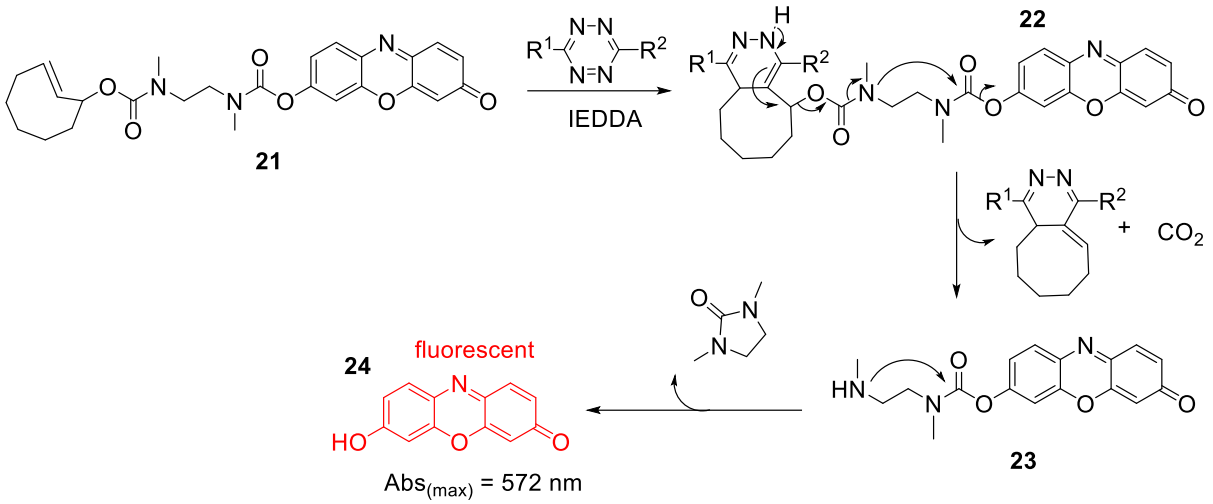

Scheme 22: Mechanism of resorufin release from TCO-Reso

The quantity and speed of the resorufin release can be measured with a UV/Vis spectrophotometer by following the increase in absorption at 572 nm, the absorption maximum of resorufin. The experiments were performed in phosphate-buffered saline (PBS, pH = 7.4) to mimic physiological environment with 1.5 equivalents of the tetrazines relative to TCO-Reso in each experiment. The data were collected for 8 h.

Three such experiments using the synthesized tetrazines were performed together with one additional experiment using dimethyl tetrazine (diMeTz) as a reference[51] (Fig. 8). Two parameters were calculated from the measured data: the observed rate constant, k_{obs}, and the approximate release (the percent of molecules released after 8 h). The observed rate constant represents the speed of the whole process (click + release) and it was calculated from the dependence of absorbance on time by fitting the observed data using the ORIGIN software.

The release was calculated from the equation (1)

$$\text{Release} = \frac{\text{Abs}_t}{\text{Abs}_{Reso}}, \qquad (1)$$

where Abs_t is the absorbance in time t and Abs_{Reso} is the absorbance of 10μM resorufin in PBS obtained before from a calibration curve.[50]

Figure 8 shows the results of the experiment for each measured tetrazine. The tetrazine-Hoechst conjugate **6** shows a release of ca. 30% after 8 hours and k_{obs} only slightly higher than that of the diMeTz. The lysosome-targeting tetrazine **7** shows a better release of ca. 42% and the k_{obs} also increased compared to **6** and diMeTz. The tetrazine-acridine conjugate **20** shows a significant increase in the k_{obs} value, though the release is at 30% after 8 hours. The results

indicate that none of the synthesized tetrazines shows a better releasing ability than diMeTz but the k_{obs} are higher for all of them which is advantageous in experiments where a quick release is necessary. The observed low release of the resorufin is probably a result of the dihydropyridazine isomerization and/or competing oxidation of the unsaturated dihydropyridazine intermediate as described previously.[52]

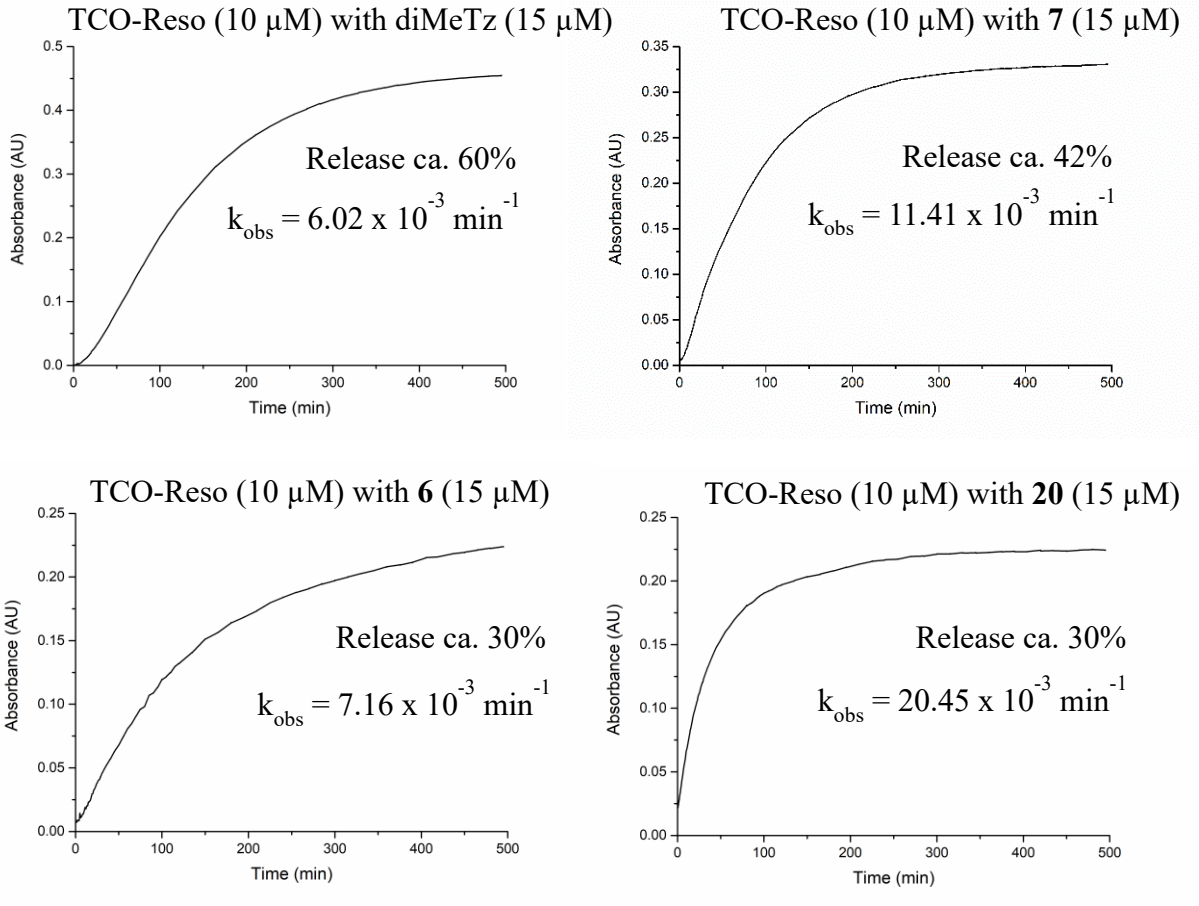

Figure 8: Measured and calculated values of k_{obs} and release from UV/Vis experiments with tetrazines

5.6 Confocal microscopy analysis of cells treated with the synthesized compounds

Using confocal microscopy performed on living cells, we examined the proper subcellular localization of the tetrazine derivatives. In the next step, we followed the release of the resorufin dye from the model TCO-Reso compound induced by the tetrazine derivatives in the cells. The experimental procedure is discussed in the chapter 6.4. For clarity, coumarin was pseudo-colored green, Hoechst is cyan and resorufin with acridine are red in the photos from confocal microscope. These experiments were performed by Dr. Dzijak.

5.6.1 Tetrazine visualization with coumarin-TCO

The goal of my thesis was to prepare tetrazine derivatives that would localize to lysosome or the nucleus. We have inspected the localization of compounds **6**, **7** and **20** using coumarin-TCO dye **14**. More specifically, live U2OS cells were incubated with 10 μM tetrazines **6**, **7** and **20** and upon wash of the free extracellular compounds, their intracellular localization was visualized by 1 μM coumarin-TCO **14**. The cells were washed again and inspected under confocal microscope.

The results (Fig. 9) show that the compound **14** has high fluorescence, with preferential localization in the lipophilic parts of the cells such as membranes. There was no difference in observed pattern between the **14** only and **14**+tetrazine conditions. This result indicates that we were unable to washout the free TOC dye from the cells. Due to that, the visualization of the tetrazines wasn't possible with this compound. A possible solution would be synthesis of other, less lipophilic TCO-dye conjugates.

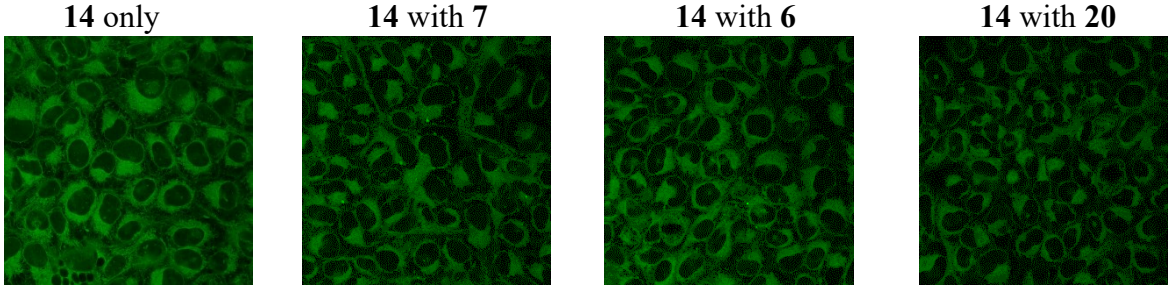

Figure 9: Coumarine-TCO derivative 14 visualization of synthesized tetrazines (6, 7 and 20)

5.6.2 Tetrazine visualization with TCO-Reso

In the next experiment (Fig. 10) we tested the potential of the prepared tetrazines to trigger the release of resorufin dye from the TCO-Reso model compound. In the first experiment, cells were incubated with 10 μM tetrazines **6**, **7** and **20** for 5 minutes and after wash, the cells were further incubated for 16 hours in the presence of 2.5 μM TCO-Reso.

Based on these results, we conclude that the releasing ability of the tetrazines in general does not seem to be very good in the living cells. The lysosome-targeting tetrazine **7** shows visible yet very small amount of resorufin fluorescence concentrated in specific spots. These spots, however, do not seem to be lysosomes. We also found that the tetrazine-acridine conjugate **20** is difficult to distinguish from the fluorescence of resorufin. In the case of the experiment with **20**, we could not evaluate the experiment because we observed fluorescence nonspecifically localized in all cells.

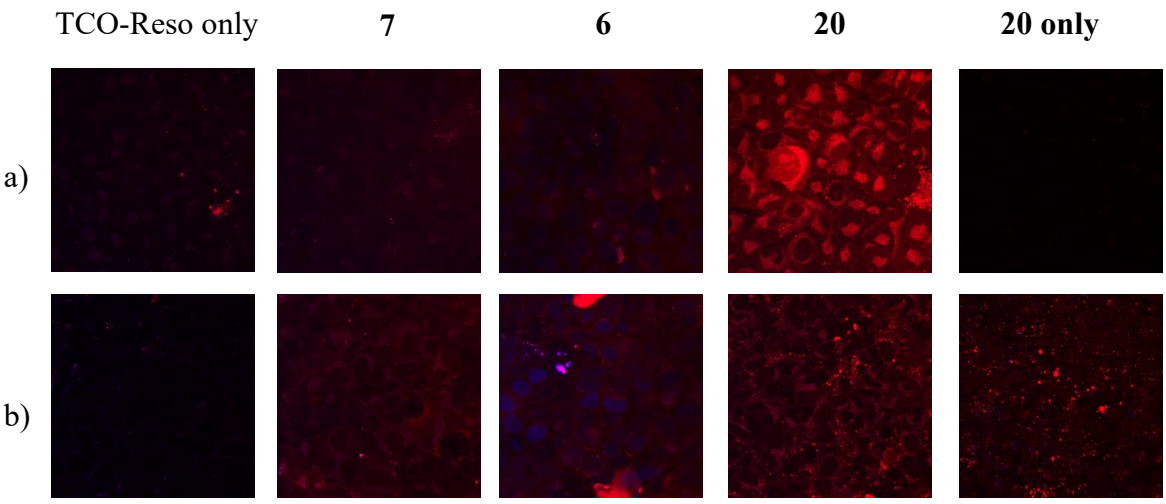

Figure 10: Tetrazines (6, 7 and 20) visualized with TCO-Reso a) right away and b) after overnight (16 h) incubation

The next experiment (Fig. 11) was performed under similar conditions to the ones shown in Fig. 10 with the difference that 5 μM TCO-Reso was added first followed by 16 h of incubation with 10 μM tetrazines. Again, we could not observe the release of resorufin. However, due to intrinsic fluorescence of the Hoechst dye, we could at least observe that the tetrazine-Hoechst **6** was accumulated in the cell nucleus. Tetrazine-Hoechst **6** is only visible in the cell nucleus in this order of adding the reagents. For some reason, it needs this order to either click with the TCO-Reso upon unquenching the fluorescence or it only gets to the nucleus when TCO-Reso is already present in the cells. The release of resorufin wasn't great as in the previous experiment, but the Hoechst fluorescence increased greatly. This points out to the fact that the tetrazine-Hoechst **6** released only small amounts of resorufin from TCO-Reso but it got its fluorescence increased only by binding to the cellular DNA (see Chapter 4.5). We can then deduce, that the tetrazine-Hoechst conjugate **6** does not have its fluorescence quenched by tetrazine as we thought it would.

The experiment with lysosome-targeting tetrazine **7** showed no resorufin or other fluorescence so it seems like this molecule does not react with TCO in the given environment and/or the resorufin release is negligible.

The fluorescence of tetrazine-acridine **20** again overlaps with the fluorescence of resorufin obstructing the interpretation of the data.

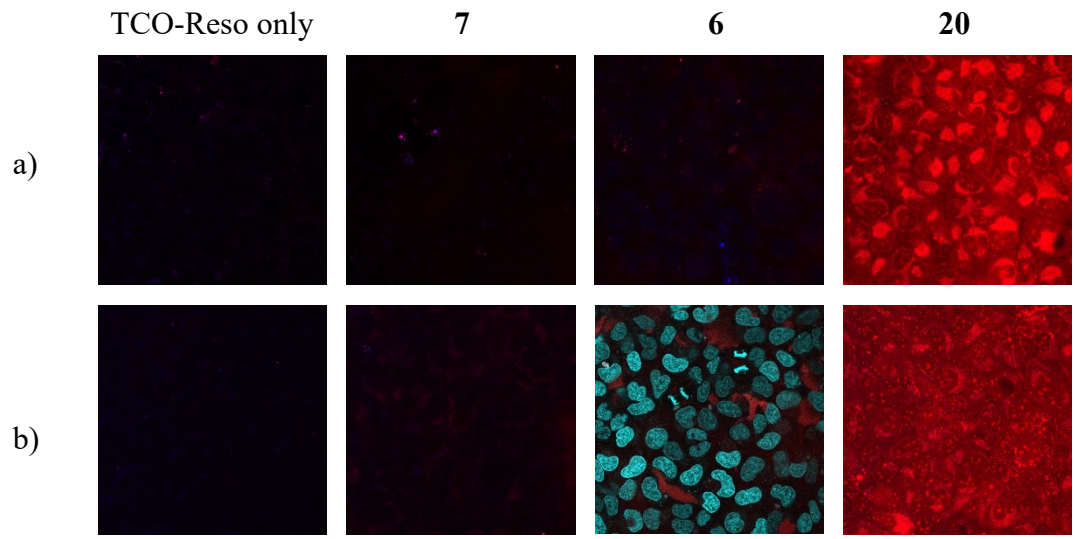

Figure 11: Repeating the experiment of visualization of tetrazines with TCO-Reso in reverse order

5.6.3 Hoechst-TCO in nuclear visualization

The previous experiments suggested that even if we could not observe tetrazine-triggered release the tetrazine-Hoechst dye **6** has the potential to accumulate properly in the nucleus. In other words, that the Hoechst can, at least to some extent, serve as nuclear-targeting moiety. To verify this, we prepared the Hoechst-TCO derivative **15** and performed the cellular localization experiment. The visualization of the Hoechst-TCO derivative **15** was performed using previously published tetrazine-coumarine derivative **GJPV503**.[46] This dye was synthesized and used in the Vrabel group for similar purposes. It has its fluorescence quenched by the tetrazine, so it becomes fluorescent when clicked with TCO (or other functional moiety that can click with tetrazines).

The first experiment was performed by incubation of cells with 10 μM of **15** followed by incubation with 1 μM **GJPV503.** The second control experiment was done with 10 μM **15** and 10 μM diMeTz. The experiment with diMeTz was performed to show that Hoechst's fluorescence in **15** is not increased by clicking the TCO moiety with a tetrazine. diMeTz was chosen because it has no intrinsic fluorescence and therefore will not interfere with the Hoechst' s fluorescence. The compound **GJPV503** unfortunately overlaps spectrally with the intrinsic fluorescence of Hoechst. Another control experiment was therefore needed using 10 μM of the compound **15** alone. The results of control experiments showed that there was similar weak fluorescence in the presence of compound **15** alone and it did not show an increase in fluorescence upon adding of diMeTz. The compound **15** however produced bright nuclear

signal in the presence of **GJPV503**. Therefore, the results in Fig. 13 show that **15** indeed accumulates in the cell nucleus and has the TCO still intact.

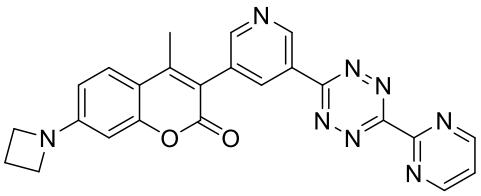

Figure 12: Structure of GJPV503

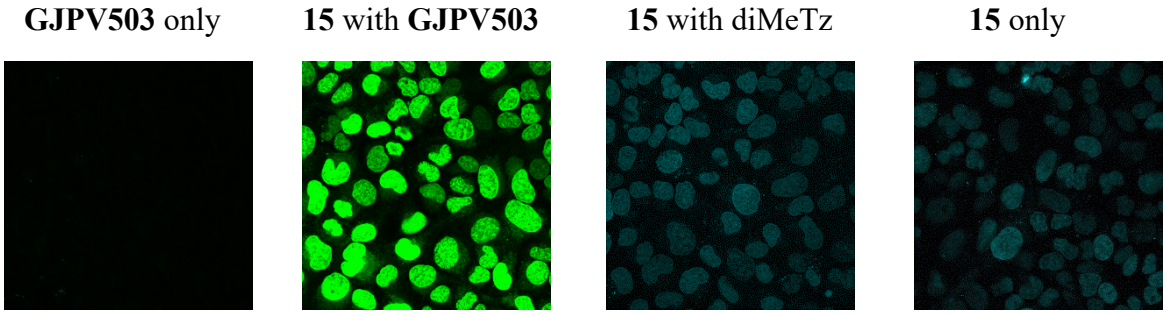

Figure 13: Hoechst-TCO derivative cellular experiments with GJPV503 (green) and diMeTz

5.6.4 Hoechst-TCO with tetrazine-acridine in nuclear visualization

The notion that the acridine tetrazine produces red fluorescent signal upon reaction with TCO prompted us to test whether it could be used to further prove the specific localization of **15**. The acridine red fluorescence is spectrally different form the Hoechst dye itself therefore it could be distinguished. This experiment was performed by first incubating the cells with 10 µM Hoechst-TCO conjugate **15** followed by the incubation with 10 µM tetrazine-acridine conjugate **20**. From the photos in Fig. 14, it is visible that both the tetrazine-acridine **20** and Hoechst-TCO **15** are accumulated in the cell nucleus where they clicked which unquenched the acridine fluorescence. The Hoechst intrinsic fluorescence could be in this case clearly distinguished from the acridine fluorescence (Fig. 14 – **15** only).

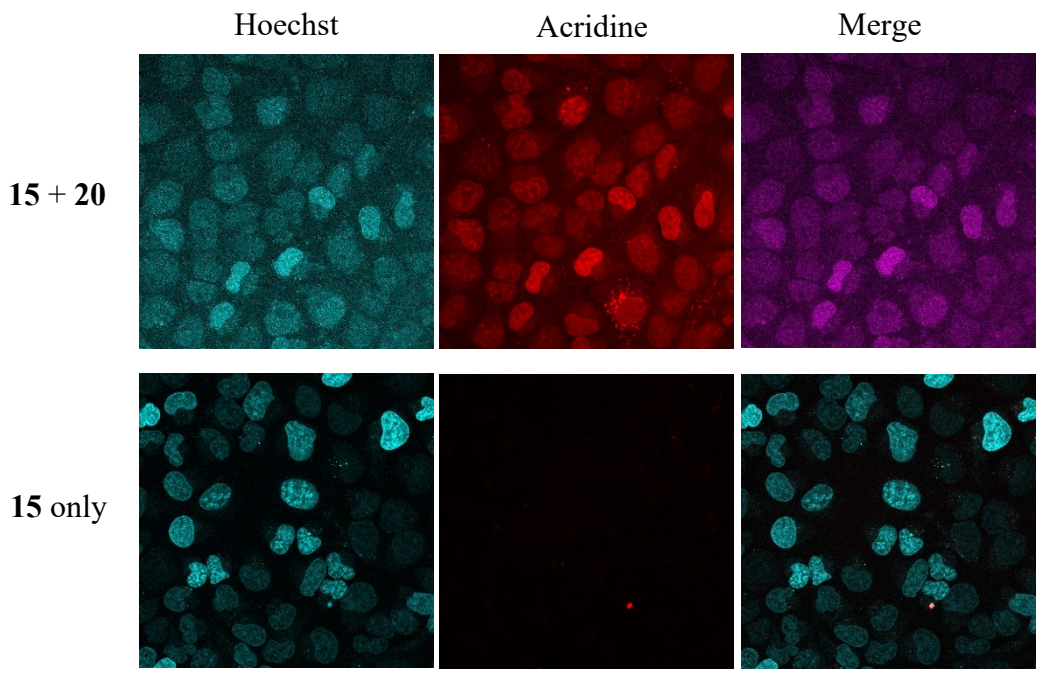

Figure 14: The initial fluorescence observed for Hoechst, acridine and the merge of the two

6. Experimental procedure

6.1 Chemicals, materials, and equipment

Solvents and other commercially available chemicals were purchased from common suppliers (Sigma-Aldrich, Fluorochem, abcr, Lach-Ner, Penta). Dry solvents were purchased from Acros Organics B.V.B.A with molecular sieves.

Reactions were monitored with TLC silica gel 60 F254 purchased from Merck. They were analyzed with a UV lamp at wavelengths 254 nm or 365 nm. Reactions were also monitored with HPLC-MS (Shimadzu LCMS-2020) in gradient of water/acetonitrile with 0.05% formic acid at the column CORTECS C18+ Column, 90 Å, 2.7 µm, 4.6 mm X 50 mm, 1/pk.

Isolation of products was performed using silica gel 40-60 µm. For reversed-phase chromatography RediSep Rf Gold® C18 columns were used. Combiflash Rf+ was used for flash column chromatography.

^{1}H an ^{13}C spectra were measured either on Bruker Avance III™ HD 400 MHz Prodigy spectrometer or on Bruker Avance III™ HD 400 MHz spectrometer. NMR assignments were done based on 1D (^{1}H, APT) and 2D (COSY, HSQC, HMBC) NMR experiments. Chemical shifts were referenced to the used solvent.

High-resolution mass spectra were recorded on Agilent 5975C MSD Quadrupol or LTQ Orbitrap XL from Thermo Fisher Scientific.

Ion exchange was performed using Dowex™ 1X8 100-200 (Cl) (Thermo Scientific™)

Evaporation of volatiles was performed with VACUUBRAND™ PC3001 VARIO™ Pro Pumping System. Lyophilization was performed using either BUCHI Lyovapor™ L-300 Freeze Dryer or FreeZone Plus 2.5 Liter Cascade Benchtop Freeze Dry System.

6.2 Synthesis of the compounds

2-(4-(6-Methyl-1,2,4,5-tetrazin-3-yl)phenyl)acetic acid (2)

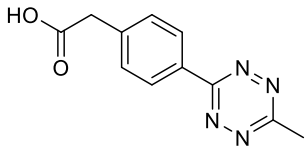

To a solution of 4-cyanophenylacetic acid **1** (6.2 mmol, 1.0 g, 1 eq.), acetonitrile (49.6 mmol, 2.6 mL, 8 eq.) and 3-mercaptopropionic acid (2.48 mmol, 216 µL, 0.4 eq.) in 2.3 mL of absolute ethanol was added hydrazine monohydrate (99.2 mmol, 4.8 mL, 16 eq.). The reaction mixture was left for stirring for 48 hours at 40°C.

The reaction mixture was cooled to 0°C in an ice-water bath and sodium nitrite (93 mmol, 6.417 g, 15 eq.) dissolved in 20 ml H_2O was added dropwise. Then, 2M HCl (aq.) was added dropwise until pH ~3 (**this step generates highly toxic nitrous gases!)**. Upon adding HCl, the reaction mixture turned pink. When the gas evolution ceased, the reaction mixture was extracted with DCM (2x 200 mL, 1x 100 mL) and the combined organic fractions were washed with brine (200 mL). The organic fraction was then dried over anhydrous Na_2SO_4, filtered and concentrated under reduced pressure. The reaction gave 790 mg of product **2** as a pink solid with 55% yield.

Spectral information in accordance with literature[42]:

2,5-Dioxopyrrolidin-1-yl 2-(4-(6-methyl-1,2,4,5- tetrazin-3-yl)phenyl)acetate (3)

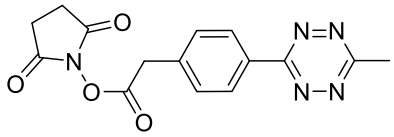

To a flask with **2** (3.43 mmol, 790 mg, 1 eq.), 30 mL of dry THF was added under argon atmosphere. The reaction mixture was cooled to 0 °C and *N*-hydroxysuccinimide (3.77 mmol, 434 mg, 1.1 eq.) was added. Then, N,N'-diisopropylcarbodiimide (DIC, 3.77 mmol, 584 µL, 1.1 eq.) was added dropwise in 5 mL of dry THF. The reaction mixture was slowly warmed to room temperature and was stirred for 20 h. The reaction was checked with TLC (DCM/AcOEt 10/1) and the product appeared as a pink spot with $R_f = 0.44$. The reaction mixture was poured to a separation funnel, 100 mL of AcOEt was added and the organic phase was washed with 100 mL of H_2O and 100 mL of brine. Organic phase was dried over anhydrous Na_2SO_4, filtered, evaporated under reduced pressure, and put on high vacuum overnight. Next day, the dried reaction mixture was mostly dissolved in DCM (white crystals of diisopropylurea byproduct are badly soluble) and loaded onto a silica column. The product was obtained with silicagel column chromatography (DCM/AcOEt 30/1 → 5/1). The reaction gave 742 mg of product **3** as a pink solid with the yield of 66%.

Spectral information in accordance with literature[42]:

***tert*-Butyl (2-(4-(6-(4-methylpiperazin-1-yl)-1H,3′H-[2,5′-bibenzo[*d*]imidazol]-2′-yl)phenoxy)ethyl)carbamate (4)**

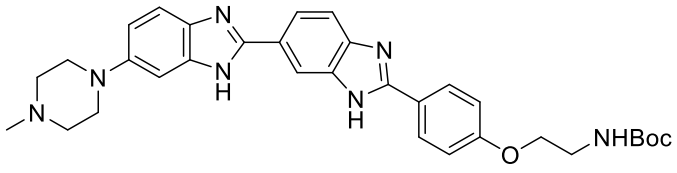

To a stirred solution of 2′-(4-hydroxyphenyl)-5-(4-methyl-1-piperazinyl)-2,5′-bi-1*H*-benzimidazole trihydrochloride (0.28 mmol, 150 mg, 1 eq.) in 2.5 mL of dry DMF, *tert*-Butyl *N*-(2-bromoethyl)carbamate (0.42 mmol, 94 mg, 1.5 eq.) in 0.5 mL of dry DMF and K_2CO_3(1.41 mmol, 195 mg, 5 eq.) were added. The reaction was stirred at 50 °C. After 2 days, HPLC-MS of the reaction mixture was measured and only a small amount of product appeared. tert-Butyl N-(2-bromoethyl)carbamate (0.22 mmol, 31.4 mg, 0.8 eq.) was added with K_2CO_3(0.28 mmol, 39 mg, 1 eq.) and the reaction mixture was stirred at 50 °C for 17 h. After that, product finally appeared. The solvents were evaporated in vacuo and the residue was purified by reverse phase flash column chromatography (0-40% acetonitrile in H_2O).

The reaction gave 47 mg of product **4** as a yellow solid with 30% yield.

^{1}H NMR (401 MHz, MeOD) δ 8.53 (s, 1H), 8.20 (d, *J* = 1.6 Hz, 1H), 8.02 – 7.97 (m, 2H), 7.90 (dd, *J* = 8.5, 1.7 Hz, 1H), 7.64 (d, *J* = 8.4 Hz, 1H), 7.49 (d, *J* = 8.8 Hz, 1H), 7.12 (d, *J* = 2.2 Hz, 1H), 7.07 – 7.03 (m, 2H), 4.04 (t, *J* = 5.6 Hz, 2H), 3.44 (t, *J* = 5.6 Hz, 2H), 3.29 (s, 2H), 3.29 (t, 4H), 3.03 (t, *J* = 5.0 Hz, 4H), 2.65 (s, 3H), 1.45 (s, 9H).

^{13}C NMR (101 MHz, MeOD) δ 162.30, 155.26, 148.87, 140.35, 135.94, 129.58, 125.40, 123.11, 122.48, 116.50, 116.09, 67.79, 55.58, 50.81, 44.88, 28.75.

ESI-HRMS: calculated for $C_{32}H_{38}N_7O_3^+$ $[M+H]^+$: 568.3031; found: 568.3031.

2-(4-(6-(4-Methylpiperazin-1-yl)-1H,3′H-[2,5′-bibenzo[*d*]imidazol]-2′-yl)phenoxy)ethan-1-amine (5)

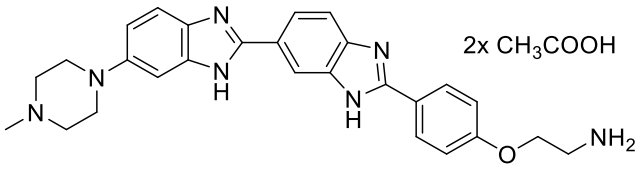

To a stirred solution of **4** in dichloromethane (0.132 mmol, 75 mg, 1 eq.) cooled to 0 °C, trifluoroacetic acid (0.5 mL, 50 eq.) was added and that the ice bath was taken away and the reaction mixture was left to stir for 1 h at room temperature. Dark brown drops of concentrated product appeared in the mixture. Volatiles were evaporated in vacuo. Ion exchange was done on Dowex (CF_3COO^- for CH_3COO^-) to be able to observe the counterions on ^{1}H NMR. The reaction gave 65 mg of product **5** as a brown solid with the yield of 84% in the form of a diacetate salt.

^{1}H NMR (400 MHz, MeOD) δ 8.23 (s, 1H), 8.09 – 8.02 (m, 2H), 7.93 (dt, *J* = 8.4, 2.0 Hz, 1H), 7.66 (dd, *J* = 8.5, 2.0 Hz, 1H), 7.49 (dd, *J* = 8.8, 2.0 Hz, 1H), 7.18 – 7.09 (m, 3H), 7.02 (dt, *J* = 8.8, 2.3 Hz, 1H), 4.30 – 4.22 (m, 2H), 3.38 – 3.31 (m, 2H), 3.27 (dt, *J* = 6.7, 2.5 Hz, 5H), 2.94 – 2.86 (m, 4H), 2.53 (d, *J* = 2.1 Hz, 3H), 1.92 (s, 6H).

^{13}C NMR (101 MHz, MeOD) δ 161.42, 155.02, 153.85, 149.14, 129.71, 126.16, 124.02, 122.62, 116.61, 116.50, 116.22, 102.65, 65.73, 55.71, 51.07, 45.20, 40.69, 28.87, 22.68.

ESI-HRMS: calculated for $C_{27}H_{30}N_7O^+$ $[M+H]^+$: 468.2506; found: 468.2505

2-(4-(6-methyl-1,2,4,5-tetrazin-3-yl)phenyl)-N-(2-(4-(6-(4-methylpiperazin-1-yl)-1H,3'H-[2,5'-bibenzo[d]imidazol]-2'-yl)phenoxy)ethyl)acetamide (6)

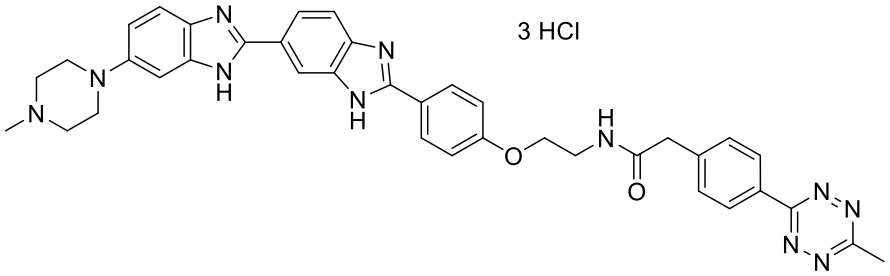

To a stirred solution of **5** (34 µmol, 20 mg, 1 eq.) in 4 mL of dry DMF, triethyl amine (68 µmol, 9.5 µL, 2 eq.) was added dropwise. Then, **3** (34 µmol, 11.5 mg, 1 eq.) was added in 2 mL of dry DMF. The reaction was stirred for 80 minutes at room temperature, and it was monitored with TLC (MeOH with 1% triethyl amine). The product was isolated with reverse phase flash column chromatography (5 – 25% of acetonitrile in H_2O). The tubes with pure product were combined and lyophilized. Ion exchange was done on Dowex (to Cl^-). The reaction gave 13 mg of product **6** as an orange solid with a 56% yield in the form of trihydrochloride.

^{1}H NMR (401 MHz, DMSO) δ 8.49 (t, J = 5.6 Hz, 1H), 8.42 – 8.36 (m, 2H), 8.27 (d, J = 5.0 Hz, 1H), 8.15 – 8.08 (m, 2H), 8.00 (dd, J = 8.4, 1.6 Hz, 1H), 7.66 (d, J = 8.7 Hz, 1H), 7.57 – 7.52 (m, 2H), 7.48 – 7.40 (m, 1H), 7.16 – 7.09 (m, 2H), 6.93 (dd, J = 8.8, 2.3 Hz, 1H), 4.13 (t, J = 5.5 Hz, 2H), 3.61 (s, 2H), 3.51 (t, J = 5.5 Hz, 1H), 3.13 (t, J = 5.0 Hz, 4H), 2.95 (s, 3H), 2.25 (s, 3H).

^{13}C NMR (101 MHz, DMSO) δ 169.99, 167.03, 163.20, 160.01, 152.72, 147.27, 141.13, 130.08, 128.23, 127.31, 124.43, 122.52, 114.95, 66.51, 54.88, 49.96, 45.77, 42.20, 38.51, 20.80.

ESI-HRMS: calculated for $C_{38}H_{38}N_{11}O_2^+$ $[M-H]^+$: 680.3204; found: 680.3210

2-(4-(6-Methyl-1,2,4,5-tetrazin-3-yl)phenyl)-*N*-(3-morpholinopropyl)acetamide (7)

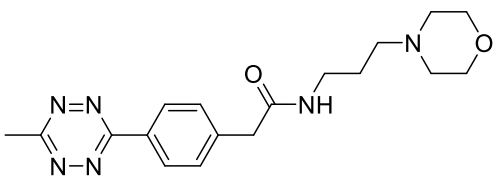

To a stirred solution of **3** (0.153 mmol, 50 mg, 1 eq.) in 3 mL of DCM cooled to 0 °C 3-morpholinopropan-1-amine (0.168 mmol, 25 µL, 1.1 eq.) and triethyl amine (0.168 mmol, 23 µL, 1.1 eq.) were added under argon atmosphere. The reaction mixture was stirred for 17 h at room temperature. HPLC-MS from the reaction mixture was measured with the product as the only significant peak. The reaction mixture was washed with 25 mL H_2O and the solvents from the organic phase were evaporated in vacuo. The reaction gave 50 mg of product **7** as a pink solid with the yield of 92%.

^{1}H NMR (401 MHz, CDCl3) δ 8.73 – 8.37 (m, 2H), 7.68 – 7.42 (m, 2H), 3.63 (s, 2H), 3.60 (t, *J* = 4.7 Hz, 4H), 3.35 (td, *J* = 6.5, 5.4 Hz, 2H), 3.09 (s, 3H), 2.43 – 2.34 (m, 6H), 1.65 (p, *J* = 6.4 Hz, 2H).

^{13}C NMR (101 MHz, CDCl3) δ 170.60, 167.44, 163.95, 140.21, 130.91, 130.28, 128.51, 67.07, 57.61, 53.82, 44.06, 39.51, 25.07, 21.30.

ESI-HRMS: calculated for $C_{18}H_{24}N_6O_2Na$: 379.1858; found: 379.18549 $[M+Na]^+$.

(4-((2-((tert-Butoxycarbonyl)amino)ethyl)carbamoyl)phenyl)boronic acid (10)

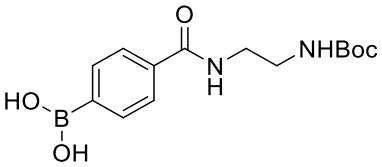

To a stirred solution of 4-carboxy-phenylboronic acid **8** (1.81 mmol, 300 mg, 1 eq.) in 4 mL of dry DMF, tert-butyl N-(2-aminoethyl)carbamate **9** (2.9 mmol, 460 µL, 1.6 eq.) was added in 2 mL dry DMF. Then, pyridine (37.97 mmol, 3.06 mL, 21 eq.) and HBTU (1.99 mmol, 754 mg, 1.1 eq.) were added. The reaction mixture was stirred for 21 h under argon atmosphere. The reaction was monitored with TLC (DCM/MeOH 9/1). The reaction mixture was washed with brine acidified with 1M HCl which resulted in precipitation of a white compound. The precipitate was filtered off and it was found to be the product using HPLC-MS and NMR. The reaction gave 370 mg of product **10** as a white solid with a 66% yield.

^{1}H NMR (401 MHz, MeOD) δ 7.78 (s, 2H), 7.69 (s, 2H), 3.46 (d, *J* = 6.9 Hz, 2H), 3.28 (s, 2H), 1.42 (s, 9H).

^{13}C NMR (101 MHz, MeOD) δ 203.31, 170.56, 159.72, 134.50, 127.65, 104.08, 80.21, 44.17, 40.83, 28.73.

ESI-HRMS: calculated for $C_{14}H_{21}N_2O_5BNa^+$: 331.1441; found: 331.1436 $[M+Na]^+$.

tert-Butyl (2-(4-(7-(diethylamino)-4-methyl-2-oxo-2H-chromen-3-yl)benzamido)ethyl) carbamate (12)

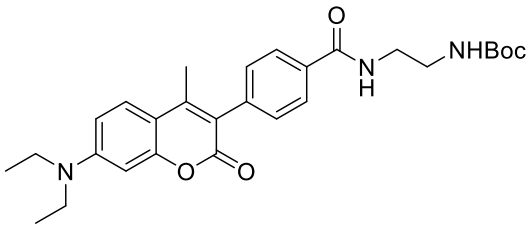

3-bromo-7-(diethylamino)-4-methyl-2H-chromen-2-one **11** (161 µmol, 50 mg, 1 eq.), Pd(dppf)Cl_2 · DCM (16 µmol, 13 mg, 0.1 eq.), **10** (322 µmol, 99 mg, 2 eq.) and K_2CO_3 (322 µmol, 44.5 mg, 2 eq.) were dissolved in 6 mL dioxane:H_2O (4:1.5) and the mixture was heated to 100 °C and left to stir for 3 h. Then, the heating was turned off and the reaction mixture was cooled to room temperature. The reaction was then extracted with DCM (3x 20 mL) and a black precipitate appeared, which was filtered over celite. The combined organic phases were checked with TLC (DCM/AcOEt 1/1) and the product was isolated using flash column chromatography (0 – 50% AcOEt in DCM). The reaction gave 36 mg of product **12** as a yellow solid with a 45% yield.

^{1}H NMR (401 MHz, CDCl3) δ 7.85 (d, *J* = 7.9 Hz, 2H), 7.45 (d, *J* = 9.0 Hz, 1H), 7.39 – 7.34 (m, 2H), 6.62 (dd, *J* = 9.0, 2.6 Hz, 1H), 6.54 (d, *J* = 2.5 Hz, 1H), 5.14 (s, 1H), 3.55 (q, *J* = 5.3 Hz, 2H), 3.42 (p, *J* = 6.7 Hz, 6H), 2.20 (s, 3H), 1.43 (s, 9H), 1.22 (t, *J* = 7.1 Hz, 6H).

^{13}C NMR (101 MHz, CDCl3) δ 167.84, 161.95, 157.45, 155.30, 150.57, 148.97, 138.80, 133.50, 130.91, 127.12, 126.32, 120.19, 109.43, 108.84, 97.53, 79.96, 44.90, 41.90, 40.27, 28.49, 16.41, 12.59.

ESI-HRMS: calculated for $C_{28}H_{35}N_3O_5Na$: 516.2474; found: 516.2469 $[M+Na]^+$

N-(2-Aminoethyl)-4-(7-(diethylamino)-4-methyl-2-oxo-2*H*-chromen-3-yl)benzamide (13)

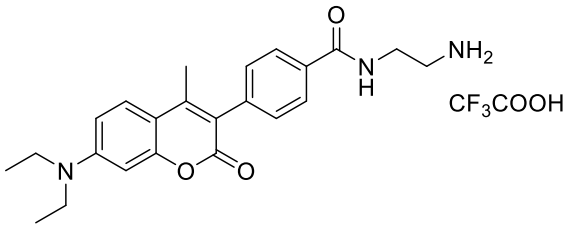

To a stirred solution of **12** (73 µmol, 36 mg, 1 eq.) in 4 ml of DCM, trifluoroacetic acid (3.65 mmol, 281 µL, 50 eq.) was added dropwise and the reaction was left to stir for 1 h at room temperature. The volatiles were evaporated, dissolved in an acetonitrile-water solution and lyophilized. The reaction gave 25 mg of product as a yellow solid with an 87% yield in the form of a trifluoroacetic salt.

^{1}H NMR (401 MHz, DMSO) δ 8.69 (t, *J* = 5.6 Hz, 1H), 7.98 – 7.90 (m, 2H), 7.90 – 7.83 (m, 2H), 7.60 (d, *J* = 9.1 Hz, 1H), 7.44 – 7.38 (m, 2H), 6.75 (dd, *J* = 9.1, 2.6 Hz, 1H), 6.56 (d, *J* =

2.5 Hz, 1H), 3.54 (q, *J* = 6.0 Hz, 2H), 3.46 (q, *J* = 7.0 Hz, 4H), 3.02 (q, *J* = 5.9 Hz, 2H), 2.19 (s, 3H), 1.14 (t, *J* = 7.0 Hz, 6H).

^{13}C NMR (101 MHz, DMSO) δ 166.71, 160.46, 154.73, 150.27, 148.80, 138.59, 132.94, 130.58, 127.02, 126.91, 118.95, 108.91, 108.43, 96.49, 44.01, 37.14, 16.13, 12.35.

ESI-HRMS: calculated for $C_{23}H_{27}N_3O_3H^+$ $[M+H]^+$: 394.2125; found: 394.2131

***trans*-Cyclooct-4-en-1-yl(2-(4-(7-(diethylamino)-4-methyl-2-oxo-2*H*-chromen-3-yl)benzamido)ethyl)carbamate (14)**

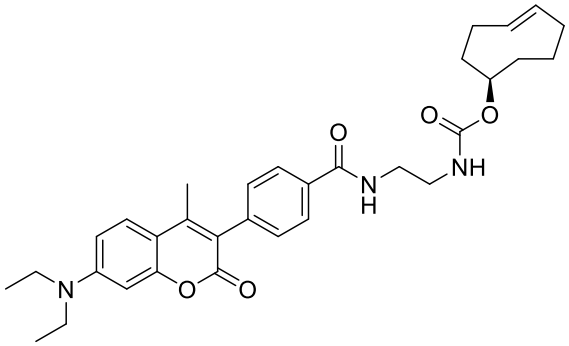

13 (19.7 µmol, 10 mg, 1 eq.), *trans*-cyclooct-4-en-1-yl (2,5-dioxopyrrolidin-1-yl) carbonate (TCO-NHS**)** (19.7 µmol, 5.27 mg, 1 eq.) and triethylamine (98.52 µmol, 13.73 µL, 5 eq.) were mixed in 2 mL of dry DMF under argon atmosphere and the reaction mixture was left for stirring at room temperature for 40 minutes. The reaction was monitored with TLC (DCM/MeOH 30/1 + 1% triethylamine). **13** was still visible on TLC, so **TCO-NHS** (2 µmol, 0.5 mg, 0.1 eq.) was added to the reaction mixture. After 30 minutes, there was no sign of **13**, reaction was finished and the volatiles were evaporated under reduced pressure. The product was purified using silica gel column chromatography (DCM/MeOH 30/1 + 1% triethylamine the whole time). The volatiles were evaporated, and the product was dissolved in an acetonitrile-water solution. The reaction gave 9 mg of product **14** appearing as a yellow fluorescent solid with an 84% yield. ^{1}H NMR showed *cis*-isomer of cyyclooctene being present. This spectrum shows protons with 4 different shifts and the approximate integrals of 0.5. Any attempt on separating the *cis*- and *trans*- isomers failed.

^{1}H NMR (400 MHz, $CDCl_3$) δ 7.85 (d, *J* = 7.8 Hz, 2H), 7.46 (dd, *J* = 9.1, 1.0 Hz, 1H), 7.41 – 7.32 (m, 2H), 7.26 (s, 1H), 7.16 (s, 1H), 6.63 (dd, *J* = 9.0, 2.6 Hz, 1H), 6.54 (d, *J* = 2.5 Hz, 1H), 5.35 (d, *J* = 4.1 Hz, 0.5H), 5.17 (s, 0.5H), 4.95 – 4.86 (m, 0.5H), 4.74 (s, 0.5H), 3.59 (dd, *J* = 14.1, 6.0 Hz, 4H), 3.43 (q, *J* = 7.1 Hz, 4H), 2.35 – 2.18 (m, 6H), 2.18 – 1.09 (m, 11H).

ESI-HRMS: calculated for $C_{32}H_{40}N_3O_5^+$ $[M-H]^+$: 546.2962; found: 546.2955

***trans*-Cyclooct-4-en-1-yl(2-(4-(6-(4-methylpiperazin-1-yl)-1*H*,3′*H*-[2,5′-bibenzo[*d*]imidazol]-2′-yl)phenoxy)ethyl)carbamate (15)**

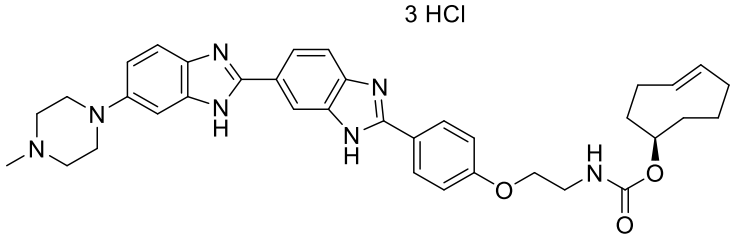

To a stirred solution of **5** (34 µmol, 20 mg, 1 eq.) in 4 mL of dry DMF, *trans*-cyclooct-4-en-1-yl (2,5-dioxopyrrolidin-1-yl) carbonate (34 µmol, 9.1 mg, 1 eq.) was added in 1 mL of DMF under argon atmosphere at room temperature. The flask was covered in an aluminum foil to prevent possible *trans*-cyclooctene photoisomerization to *cis*. Then, triethylamine (170 µmol, 24 µL, 5 eq.) was added to the reaction mixture and it was stirred for 1.5 h. The reaction was monitored with TLC ($CHCl_3$/MeOH 1/1 + 1% triethylamine) and a visible spot corresponding to **5** appeared. *trans*-Cyclooct-4-en-1-yl (2,5-dioxopyrrolidin-1-yl) carbonate (3.5 µmol, 1 mg, 0.1 eq.) was added and after another 40 min, the starting compound was no longer present. The volatiles were evaporated in vacuo and to the solid mixture was added toluene (2 ml) and evaporated under reduced pressure to get rid of trace amount of DMF. The product was purified using flash column chromatography (DCM/MeOH 20/1 to 5/1 + 1% triethylamine). The phases containing product were combined and the volatiles were evaporated in vacuo. The product was dissolved in water/acetonitrile solution and lyophilized. The reaction gave 16 mg of product as a yellow-brown solid with an 80% yield in the form of a trihydrochloride.

^{1}H NMR (401 MHz, MeOD) δ 8.17 (d, *J* = 1.7 Hz, 1H), 8.01 – 7.93 (m, 2H), 7.88 (dd, *J* = 8.5, 1.7 Hz, 1H), 7.61 (d, *J* = 8.5 Hz, 1H), 7.45 (d, *J* = 8.7 Hz, 1H), 7.08 (d, *J* = 2.2 Hz, 1H), 7.04 – 7.00 (m, 2H), 6.98 (dd, *J* = 8.8, 2.2 Hz, 1H), 5.70 – 5.43 (m, 1H), 5.17 (s, 1H), 4.04 (t, *J* = 5.6 Hz, 2H), 3.50 – 3.35 (m, 4H), 3.28 (p, *J* = 1.6 Hz, 2H), 3.24 – 3.19 (m, 4H), 3.14 (q, *J* = 7.3 Hz, 1H), 2.81 (t, *J* = 4.9 Hz, 4H), 2.47 (s, 3H), 2.36 – 1.17 (m, 9H).

^{13}C NMR (101 MHz, MeOD) δ 162.30, 158.77, 155.17, 153.10, 149.17, 140.20, 136.35, 132.14, 129.05, 126.18, 123.12, 122.46, 121.76, 117.14, 116.38, 116.09, 102.49, 71.56, 68.02, 63.02, 55.83, 53.98, 51.24, 48.79, 41.30, 35.24, 33.72, 30.46, 28.98.

6-(Dimethylamino)acridine-3-carbonitrile (19)

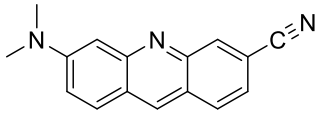

A flask containing *N*,*N*-dimethylbenzene-1,3-diamine **16** (463 µmol, 63 mg, 1 eq.), 1,1′-Ferrocenediyl-bis(diphenylphosphine) (23 µmol, 12.8 mg, 0.05 eq.), Tris(dibenzylideneacetone)dipalladium(0) (11.6 µmol, 10.6 mg, 0.025 eq.) and K_2CO_3 (925 µmol, 128 mg, 2 eq.) was evacuated for 10 min and flushed with argon. Then, 3-bromo-4-formylbenzonitrile **17** (555 µmol, 117 mg, 1.2 eq.) was added in 1.9 mL of toluene. The reaction mixture was heated to 80 °C and was left to stir for 17 h. Then, the reaction was cooled to room temperature and roughly 1.5 mL of silica gel was added to the reaction mixture, and it was left to stir for 1 h. The reaction mixture changed color from yellow to red. Then, the reaction mixture was concentrated under reduced pressure and the product was purified using silica gel column chromatography (EtOAc/petroleum ether 1/1). The reaction gave 26 mg of product **19** as a red solid with a 23% yield. Spectral information were in accordance with literature.[48]

***N*,*N*-dimethyl-6-(6-methyl-1,2,4,5-tetrazin-3-yl)acridin-3-amine (20)**

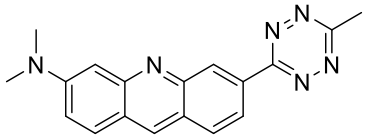

To flask containing **19** (105 µmol, 26 mg, 1 eq.), hydrazine (1M in THF, 5.3 mmol, 5.3 mL, 50 eq.) and acetonitrile (1.05 mmol, 55 µL, 10 eq.) were added. Then Zinc(II) trifluoromethanesulfonate (52 µmol, 19.11 mg, 0.5 eq.) was added and the reaction was stirred at 60 °C for 5 days. The flask was closed with a lid and parafilmed in order to avoid the evaporation of acetonitrile. The reaction mixture was cooled to room temperature and $NaNO_2$ (1.63 mmol, 113 mg, 15.5 eq.) was added and the reaction mixture was acidified with 6M HCl to pH ~3. The reaction mixture was left for stirring until the gas evolution ceased. The reaction was monitored with TLC (DCM/MeOH 10/1). The reaction mixture was extracted with DCM (6x 20 mL), the organic phases were combined, and the volatiles were evaporated under reduced pressure. (We don't recommend drying over $MgSO_4$ because the product seems to stick to it). The product was purified with silica gel column chromatography (DCM/MeOH 30/1) but the product still contained impurities. Second column was done in DCM/MeOH 100/1 – 50/1. ^{1}H NMR in $CDCl_3$ was measured but the product still wasn't pure. A reverse phase flash column chromatography was used twice subsequently (both 5 – 40% acetonitrile in H_2O). The reaction gave 2.8 mg of product **20** as a red solid an 8% yield. Spectral information were in accordance with literature.[48]

^{1}H NMR (400 MHz, CDCl3) δ 9.44 (s, 1H), 8.62 (s, 1H), 8.57 – 8.46 (m, 1H), 8.10 (d, *J* = 8.7 Hz, 1H), 7.87 (d, *J* = 9.4 Hz, 1H), 7.35 (dd, *J* = 9.4, 2.5 Hz, 1H), 7.25 (d, 1H), 3.22 (s, 6H), 3.14 (s, 3H).

6.3 Tetrazine with TCO-Reso decaging experiment

To a solution of TCO-Reso (10 μM final concentration) in PBS containing 5% DMSO (3 mL total volume) was added a solution of the respective tetrazine (1.5 equiv. from 10 mM stock in DMSO). The cuvettes were inserted into UV/Vis spectrophotometer and the measurement was started. The increasing concentration of the released resorufin was monitored at 575 nm over 8 hours. 10 μM solution of TCO-Reso in PBS containing 5% DMSO was used as blank. The results from this experiment are shown in Figure 8 in the main text. The experimental procedure was done according to a 2020 article.[50]

6.4 Confocal microscopy analysis of cells treated with the synthesized compounds

The experiments were performed on U-2 OS cell line. Cells were cultivated in DMEM cultivation media with the addition of 10 μL fetal bovine serum. In each experiment, the cultivation media was replaced with media containing the examined compounds in a specific concentration. The photos were taken using a confocal microscope.

6.4.1 Tetrazine visualization with coumarin-TCO

The cells were treated with 10 μM tetrazines **6**, **7**, **20** in 100 μL of cultivation media in three separate experiments. After 5 min of incubation, the cells were washed 2x with fresh cultivation media followed by the addition of 1 μM Hoechst-Tetrazine conjugate **14** in 100 μL of cultivation media. After a 5 min incubation, the cells were washed 3x with the media and photos (Figure 9) was taken using a confocal microscope.

6.4.2 Tetrazine visualization with TCO-Reso

The cells were treated with 10 μM tetrazines **6**, **7**, **20** in 100 μL of cultivation media. After 1 min incubation, the cells were washed with fresh media. Then 2.5 μM TCO-Reso (**21**) in 100 μL of cultivation media was added. The photos were taken using a confocal microscope (Fig. 10 and Fig. 11). Then, the same experiment was repeated but 5 μM TCO-Reso (**21**) in 100 μL of cultivation media was added first followed by the addition of the respective tetrazines.

6.4.3 Hoechst-TCO in nuclear visualization

The cells were treated with 10 μM Hoechst-TCO **15** in 100 μL of cultivation media. Then the media was replaced with 100 μL of media containing 1 μM **GJPV-503** in one experiment or 10 μM diMeTz in the other. The photos (Fig. 13) were taken using a confocal microscope. The dyes were excited using 405 nm excitation wavelength and the fluoreresecence was collected in 410-694 nm interval. In each condition, the setup of laser intensity and detector sensitivity was identical.

6.4.4 Hoechst-TCO with tetrazine-acridine in nuclear visualization

The cells were treated with 10 μM Hoechst-TCO **15** in 100 μL of cultivation media. After 10 min of incubation, the media was replaced with 100 μL of media containing 10 μM tetrazine-acridine conjugate **20**. The cells were washed 1x with cultivation media. The photos (Fig. 14) were taken using a confocal microscope. The Hoechst dye was excited with 405 nm laser and the fluorescence was collected in 410-490 nm interval. The acridine fluorescence was excited using 488nm laser and the emission recorded in 570-694 nm interval.

7. Conclusion

Based on literature research, new derivatives of tetrazines and TCOs with potential affinity to the cell nucleus or lysosomes were designed and synthesized. In total, five final products were isolated, namely three tetrazine derivatives **6**, **7** and **20** and two TCO derivatives **14** and **15**. These molecules were characterized using NMR spectroscopy and HRMS.

The tetrazines were tested for their ability to release fluorogenic resorufin from an allyl substituted TCO-dye conjugate (TCO-Reso). The rate of the release of the candidate tetrazines was measured in contrast to diMeTz as the observed rate constant k_{obs}. It was found that all candidate tetrazines release with higher k_{obs} than diMeTz. On the other hand, diMeTz had a higher value of the overall release than all the candidate tetrazines after 8 hours of measurements. These experiments indicate the potential use of the prepared tetrazine derivatives in experiments where fast burst of the released compound is desirable.

A series of experiments was performed on U-2 OS cells. First, the tetrazines **6**, **7** and **20** were tested for their desired properties – **7** for its affinity to lysosomes and **6** with **20** for their affinity to the cell nucleus. The tetrazines were visualized in the cells using coumarin-TCO derivative **14** which led to no concrete conclusions because **14** binds nonspecifically in lipophilic regions of the cells without properly visualizing the tetrazines.

The next experiment was performed to test the releasing ability of the candidate tetrazines, this time using fluorogenic precursor TCO-Reso. It seems like in general, the tetrazines don't possess a good ability to release from TCO in the cells, because only trace amounts of released resorufin were observed. On the other hand, it was found that tetrazine-Hoechst **6** accumulated in the cell nucleus.

Subsequently, Hoechst-TCO **15** was tested to clarify the targeting ability of the Hoechst moiety. It was found that it has a rather weak intrinsic fluorescence (when compared to 'standard' Hoechst dye), but it was visualized with a fluorogenic tetrazine-coumarin conjugate **GJPV-503** to find that it actually is accumulated in the cell nucleus.

This property of Hoechst-TCO **15** was further addressed in an experiment where the cells were treated with **15** and **20** to find out if these two compounds click together while unquenching the fluorescence of acridine and therefore if they are able to visualize the cell nucleus. The experiment confirmed the hypothesis and both acridine and Hoechst fluorescence was observed specifically in the nucleus of the cells. This means, that the Hoechst-TCO **15** could serve as a potential model molecule for prodrugs with an affinity to the nucleus.

The tetrazine-acridine **20** had its fluorescence successfully unquenched in the last experiment and it therefore could serve for visualization of TCOs in the cells. The affinity of **20** to the cell nucleus wasn't observed but it might have an affinity to other subcellular compartments (possibly lysosomes).

Based on these results we conclude that targeting cellular nucleus using Hoechst as the targeting moiety is feasible however, even small structural changes may have great impact on localization of the compounds and good control experiments are needed to verify the 'real' localization in the cells. For the intended nuclear-specific drug release application, one would need to optimize the releasing ability of the tetrazine compounds as well.

7. Acknowledgements

I would like to thank my advisor, Mgr. Michal Rahm, for his guidance throughout the year I spent at IOCB. I would like to express my feeling of gratitude for his patience and advice in numerous difficult situations. My thanks also belong to my supervisor and group leader, Ing. Milan Vrábel Ph.D., for taking me in the group at IOCB knowing I have very little experience in the field. He was always there to consult me on my scientific work. Next, I'd like to thank my colleague, Ing. Rastislav Dzijak Ph.D., for performing the cellular testing on my compounds and for consulting me on the results. Also, I want to thank all my colleagues at IOCB who made the pleasant environment I had the pleasure of working in.

I thank my family for their unconditional support in my years as a student. Without them I never would have made it.

8. References

(1) Bird, R. E.; Lemmel, S. A.; Yu, X.; Zhou, Q. A. *Bioconjug. Chem.* **2021**, *32 (12)*, 2457–2479.

(2) Blackman, M. L.; Royzen, M.; Fox, J. M. *J. Am. Chem. Soc.* **2008**, 130(41), 13518-13519.

(3) Oliveira, B. L.; Guo, Z.; Bernardes, G. J. L. *Chemical Society Reviews*. **2017**, 46, 4895-4950

(4) Neumann, K.; Gambardella, A.; Bradley, M. *ChemBioChem* **2019**, 20 (7) 872-876.

(5) Sakhrani, N. M.; Padh, H. *Drug Design, Development and Therapy*. **2013**. 7, 585-599.

(6) Scinto, S. L.; Bilodeau, D. A.; Hincapie, R.; Lee, W.; Nguyen, S. S.; Xu, M.; am Ende, C. W.; Finn, M. G.; Lang, K.; Lin, Q.; Pezacki, J. P.; Prescher, J. A.; Robillard, M. S.; Fox, J. M. *Nat. Rev. Methods Prim.* **2021**, *1* (1), 1–23.

(7) Saxon, E.; Bertozzi, C. R. *Science (80-.).* **2000,** 287 (5460), 2007-2010.

(8) Kiick, K. L.; Saxon, E.; Tirrell, D. A.; Bertozzi, C. R. *Proc. Natl. Acad. Sci. U. S. A.* **2002**, 99 (1) 19-24.

(9) Osako, T.; Uozumi, Y.; Osako, T.; Uozumi, Y. *Synlett* **2015**, *26*, 1475–1479.

(10) Gutmann, M.; Memmel, E.; Braun, A. C.; Seibel, J.; Meinel, L.; Lühmann, T. *ChemBioChem* **2016**, 17 (9), 866-875.

(11) Ojida, A.; Tsutsumi, H.; Kasagi, N.; Hamachi, I. *Tetrahedron Lett.* **2005**, 46 (19), 3301-3305.

(12) Lin, Y. A.; Chalker, J. M.; Floyd, N.; Bernardes, G. J. L.; Davis, B. G. *J. Am. Chem. Soc.* **2008**, 130 (30), 9642-9643.

(13) Rostovtsev, V. V.; Green, L. G.; Fokin, V. V.; Sharpless, K. B. *Angew. Chemie - Int. Ed.* **2002**, 41 (14), 2596-2599

(14) Tornøe, C. W.; Christensen, C.; Meldal, M. *J. Org. Chem.* **2002**, 67, 9, 3057–3064

(15) Dommerholt, J.; Rutjes, F. P. J. T.; van Delft, F. L. *Topics in Current Chemistry*. **2016**, 374(16), 1-20.

(16) Ji, X.; Pan, Z.; Yu, B.; De La Cruz, L. K.; Zheng, Y.; Ke, B.; Wang, B. *Chemical Society Reviews*. **2019**, 48, 1077-1094

(17) Rossin, R.; Van Duijnhoven, S. M. J.; Ten Hoeve, W.; Janssen, H. M.; Kleijn, L. H. J.; Hoeben, F. J. M.; Versteegen, R. M.; Robillard, M. S. *Bioconjug. Chem.* **2016**, 27 (7), 1697–1706.

(18) Rossin, R.; Versteegen, R. M.; Wu, J.; Khasanov, A.; Wessels, H. J.; Steenbergen, E. J.; Ten Hoeve, W.; Janssen, H. M.; Van Onzen, A. H. A. M.; Hudson, P. J.; Robillard, M. S. *Nat. Commun.* **2018**, 9 (1484), 1-11.

(19) Oneto, J. M. M.; Khan, I.; Seebald, L.; Royzen, M. *ACS Cent. Sci.* **2016,** 2 (7), 476–482.

(20) Neumann, K.; Gambardella, A.; Lilienkampf, A.; Bradley, M. *Chem. Sci.* **2018**, 9, 7198-7203.

(21) Friedman, J. R.; Nunnari, J. *Nature*. **2014**, 505, 335–343

(22) Kim, J. W.; Dang, C. V. *Cancer Research*. **2006**, 66 (18), 8927-8930.

(23) Wang, F.; Zhang, Y.; Liu, Z.; Du, Z.; Zhang, L.; Ren, J.; Qu, X. *Angew. Chemie - Int. Ed.* **2019**, 58 (21), 6987-6992.

(24) Hoogewijs, K.; James, A. M.; Smith, R. A. J.; Gait, M. J.; Murphy, M. P.; Lightowlers, R. N. *ChemBioChem* **2016**, 17 (14), 1312-1316.

(25) Zheng, Y.; Ji, X.; Yu, B.; Ji, K.; Gallo, D.; Csizmadia, E.; Zhu, M.; Choudhury, M. R.; De La Cruz, L. K. C.; Chittavong, V.; Pan, Z.; Yuan, Z.; Otterbein, L. E.; Wang, B. *Nat. Chem.* **2018**, 10, 787-794.

(26) Smith, R. A. J.; Porteous, C. M.; Coulter, C. V.; Murphy, M. P. *Eur. J. Biochem.* **1999**, 263 (3), 709-716.

(27) Lübke, T.; Lobel, P.; Sleat, D. E. *Biochimica et Biophysica Acta - Molecular Cell Research*. **2009**, 1793 (4), 625-635

(28) Bagshaw, R. D.; Mahuran, D. J.; Callahan, J. W. *Mol. Cell. Proteomics* **2005**, 4 (2), 133-143.

(29) Ni, X.; Canuel, M.; Morales, C. R. *Histology and Histopathology*. **2006**, 21, 899-913.

(30) Sly, W. S.; Vogler, C. *Proc. Natl. Acad. Sci. U. S. A.* **2002**, 99 (9), 5760-5762.

(31) Olsson, M.; Rundquist, I.; Brunk, U. *Acta Pathol. Microbiol. Scand. Ser. A Pathol.* **1987**. 95A (1-6), 159-165.

(32) Wang, Y.; Li, J.; Feng, L.; Yu, J.; Zhang, Y.; Ye, D.; Chen, H. Y. *Anal. Chem.* **2016**, 88 (24), 12403-12410.

(33) Aridor, M.; Hannan, L. A. Tarffic Jam: *Traffic* **2000**, *1* (11), 836–851.

(34) Boelens, J.; Lust, S.; Offner, F.; Bracke, M. E.; Vanhoecke, B. W. *In Vivo*. **2007**, 21(2), 215-226.

(35) Phaniraj, S.; Gao, Z.; Rane, D.; Peterson, B. R. *Dye. Pigment.* **2016**, 135, 127-133.

(36) Louzoun-Zada, S.; Jaber, Q. Z.; Fridman, M. *Angewandte Chemie - International Edition*. **2019**, 58 (44), 15584-15594

(37) Bucevičius, J.; Lukinavičius, G.; Gerasimaite, R. *Chemosensors*. **2018**, 6(2), 18

(38) Han, F.; Taulier, N.; Chalikian, T. V. *Biochemistry* **2005**, 44 (28), 9785-9794.

(39) Wagner, M.; Weber, P.; Bruns, T.; Strauss, W. S. L.; Wittig, R.; Schneckenburger, H. *Int. J. Mol. Sci.* **2010**, 11 (3), 956-966.

(40) Dasari, M.; Lee, S.; Sy, J.; Kim, D.; Lee, S.; Brown, M.; Davis, M.; Murthy, N. *Org. Lett.* **2010**, 12 (15), 3300-3303.

(41) Dasari, M.; Acharya, A. P.; Kim, D.; Lee, S.; Lee, S.; Rhea, J.; Molinaro, R.; Murthy, N. *Bioconjug. Chem.* **2013**, 24 (1), 4-8.

(42) La–Venia, A.; Dzijak, R.; Rampmaier, R.; Vrabel, M. *Chem. - A Eur. J.* **2021**, 27 (54), 13632-13641.

(43) Ramadoss, N. S.; Schulman, A. D.; Choi, S. H.; Rodgers, D. T.; Kazane, S. A.; Kim, C. H.; Lawson, B. R.; Young, T. S. *J. Am. Chem. Soc.* **2015**, 137 (16), 5288-5291.

(44) Mao, W.; Shi, W.; Li, J.; Su, D.; Wang, X.; Zhang, L.; Pan, L.; Wu, X.; Wu, H. *Angew. Chemie - Int. Ed.* **2019**, 58 (4), 1106-1109.

(45) Kozma, E.; Demeter, O.; Kele, P. Bio-Orthogonal Fluorescent Labelling of Biopolymers through Inverse-Electron-Demand Diels–Alder Reactions. *ChemBioChem*. **2017**, 18 (6), 486-501.

(46) Galeta, J.; Dzijak, R.; Obořil, J.; Dračínský, M.; Vrabel, M. *Chem. - A Eur. J.* **2020**, 26 (44), 9945-9953

(47) Fang, Y.; Judkins, J. C.; Boyd, S. J.; am Ende, C. W.; Rohlfing, K.; Huang, Z.; Xie, Y.; Johnson, D. S.; Fox, J. M. *Tetrahedron* **2019**, 75 (32), 4307-4317.

(48) Loehr, M. O.; Luedtke, N. W. *Angew. Chemie Int. Ed.* **2022**, 1-5.

(49) Jun, J. V.; Petersson, E. J.; Chenoweth, D. M. *J. Am. Chem. Soc.* **2018**, 140 (30), 9486–9493.

(50) Mancuso, F.; Rahm, M.; Dzijak, R.; Mertlíková-Kaiserová, H.; Vrabel, M. *Chempluschem* **2020**, 85 (8), 1669-1675.

(51) Versteegen, R. M.; Rossin, R.; Ten Hoeve, W.; Janssen, H. M.; Robillard, M. S. *Angew. Chemie - Int. Ed.* **2013**, 52 (52), 14112-14116.

(52) Carlson, J. C. T.; Mikula, H.; Weissleder, R. *J. Am. Chem. Soc.* **2018**, 140 (10), 3603–3612.